# Statistical and machine learning methods for evaluating trends in air quality under changing meteorological conditions

**Minghao Qiu[1], Corwin M. Zigler[2], and Noelle E. Selin[1,3]**

[1]Institute for Data, Systems, and Society, Massachusetts Institute of Technology
[2]Departments of Statistics and Data Science and Women's Health, University of Texas, Austin
[3]Department of Earth, Atmospheric, and Planetary Sciences, Massachusetts Institute of Technology

**Key Points:**

- Widely-used regression methods perform poorly in correcting for meteorology variability and estimating emission-driven trend of air quality.
- We propose a model using local and regional scale meteorological features with better performance than typically-used regression models.
- We quantify the degree to which separately attributing trends in pollution to emission and meteorology is possible and the associated error.

Corresponding author: Minghao Qiu, mhqiu@mit.edu

**Abstract**

Evaluating the influence of anthropogenic emissions changes on air quality requires accounting for the influence of meteorological variability. Statistical methods such as multiple linear regression (MLR) models with basic meteorological variables are often used to remove meteorological variability and estimate trends in measured pollutant concentrations attributable to emissions changes. However, the ability of these widely-used statistical approaches to correct for meteorological variability remains unknown, limiting their usefulness in the real-world policy evaluations. Here, we quantify the performance of MLR and other quantitative methods using two scenarios simulated by a chemical transport model, GEOS-Chem, as a synthetic dataset. Focusing on the impacts of anthropogenic emissions changes in the US (2011 to 2017) and China (2013 to 2017) on $PM_{2.5}$ and $O_3$, we show that widely-used regression methods do not perform well in correcting for meteorological variability and identifying long-term trends in ambient pollution related to changes in emissions. The estimation errors, characterized as the differences between meteorology-corrected trends and emission-driven trends under constant meteorology scenarios, can be reduced by 30%-42% using a random forest model that incorporates both local and regional scale meteorological features. We further design a correction method based on GEOS-Chem simulations with constant emission input and quantify the degree to which emissions and meteorological influences are inseparable, due to their process-based interactions. We conclude by providing recommendations for evaluating the effectiveness of emissions reduction policies using statistical approaches.

## 1 Introduction

Researchers and policy makers have long been interested in understanding the anthropogenic drivers of trends in observed air pollutant concentrations in order to inform air quality policies. Declining trends in pollutant concentrations such as particulate matter with diameter less than 2.5 microns ($PM_{2.5}$) have been observed in many countries that adopted policies to limit anthropogenic emissions such as $SO_2$ and $NO_x$, including the US (McClure & Jaffe, 2018) and China (Q. Zhang et al., 2019). As information on anthropogenic emissions are often unavailable or very uncertain, researchers and policy makers often rely on the trends in measured air pollutants to assess the effects of polices. Evaluating the effectiveness of air quality policies requires understanding the degree to which changing trends in observed concentrations can be attributed to anthropogenic emissions changes. However, rigorous attribution requires correcting for the influence of changing meteorology, which has become increasingly important but challenging in a changing climate (Saari et al., 2019). Numerous papers attempt to use statistical methods to separate impacts of meteorology from emissions changes in evaluating trends in air quality, but the performances of these commonly-used statistical approaches remain unassessed. Further, the impacts of meteorological variability may not even be distinguishable from emissions-driven air quality trends, due to their interactions; the magnitude of this interaction also remains unquantified. In this paper, we devise a model-based experiment for evaluating the performance of different statistical methods used for meteorological corrections. We focus on a case of identifying emissions-driven linear trends in measured concentrations of $PM_{2.5}$ and ozone ($O_3$), when information on the anthropogenic emission is not available.

Measured pollutant concentrations are often used as the primary basis for evaluating air quality actions. For example in 2013, China's central government established targets that aimed to reduce annual average $PM_{2.5}$ concentrations of three urban clusters by 15% to 25% between 2012 and 2017 (State Council of the People's Republic of China, 2013). This later translated into a stringent and binding target of a maximum annual mean $PM_{2.5}$ concentration of 60 $\mu g/m^3$ in 2017 for Beijing, which was ultimately reached (the 2017 concentration was 58.5 $\mu g\ m^{-3}$) (Beijing Municipal Ecology and Environment Bureau, 2013). However, several studies estimated that the concentration would

have exceeded this target in Beijing were it not for meteorological conditions in winter 2017 that favored pollution reductions (Vu et al., 2019; Z. Chen et al., 2019; Cheng et al., 2019). The European Union and US Environmental Protection Agency (EPA) use a three-year average of the $PM_{2.5}$ concentration to determine compliance with air quality standards (European Union, 2020; U.S. Environmental Protection Agency, 2019). The US EPA has also proposed to use statistical approaches that aim to correct for the impacts of weather variability on $O_3$ concentrations in the designation processes (Wells et al., 2021).

Many studies use multiple linear regression (MLR) models with basic meteorological variables to correct for meteorological variability in order to estimate the impacts of emissions changes on measured air quality (Otero et al., 2018; Zhai et al., 2019; K. Li et al., 2018, 2020; Han et al., 2020; L. Chen et al., 2020). Zhai et al. (2019) and K. Li et al. (2020) use MLR models to estimate the degree to which trends in $PM_{2.5}$ and $O_3$ from 2013 to 2019 in China were driven by anthropogenic emissions changes. They first use MLR to predict the $PM_{2.5}$ and $O_3$ concentrations with meteorological variables, and then interpret the residuals of the MLR model as signals resulting from emissions changes. A related approach is to combine MLR with techniques that can decompose time series of observed concentrations into long-term, seasonal, and short-term components (e.g., Kolmogorov-Zurbenko (KZ) filters (Zurbenko, 1994)). Ma et al. (2016) and Z. Chen et al. (2019) use KZ filters to calculate the long-term component of observed $PM_{2.5}$ and then apply MLR to separate the impacts of long-term meteorological changes on the concentrations. Henneman et al. (2015) apply MLR to the short-term component (identified by KZ filters) of air pollutant concentrations near Atlanta during 2000 to 2012, to separate the impact of short-term meteorological variability, and then estimate the long-term trend in air quality.

Other statistical methods including non-linear regression or machine learning models have also been used to correct for meteorological variability (Holland et al., 1998; Carslaw et al., 2007; Hayn et al., 2009; Vu et al., 2019). One popular method is to use a generalized additive model (GAM) to estimate non-linear smooth functions of each meteorological variable within a given smoothing function family with penalization on non-smoothness. The US EPA uses a GAM model of temperature, wind direction and speed, humidity, pressure, stability, transport trajectories, and synoptic weather to perform weather corrections in assessing long term trends in $O_3$ (Camalier et al., 2007). An increasing number of studies use machine learning models (Grange et al., 2018; Vu et al., 2019; Y. Zhang et al., 2020; Shi et al., 2021; Qu et al., 2020). Vu et al. (2019) uses a random forest model to predict pollutant concentrations in Beijing with time index and meteorological variables and then calculates the "weather-normalized" concentration for each day with 1000 sets of meteorological fields drawn from the historical meteorological data. They found that the decrease of $PM_{2.5}$ during 2013 to 2017 was largely driven by emissions reductions, although the magnitude of reduction is smaller when correcting for the meteorological variability.

Despite the large amount of papers which apply various meteorology correction methods, very little is known about whether these methods can effectively correct for meteorological variability and thus reveal the underlying causal impacts of anthropogenic emissions changes. Most studies cite the prediction performance of their statistical models (such as $R^2$ and/or mean squared errors) to justify their method choice and analysis. However, good prediction performance does not guarantee correct inference of causal effects (Runge et al., 2019). The performance of these meteorology-corrected methods is unable to be assessed using observational data alone, as the underlying emission-driven trends without influence from meteorological variability cannot be derived from data. Runge et al. documents similar challenges with observational data and proposes to use physical models to benchmark causal inference methods in the broader domains of earth sciences (Runge et al., 2019). Further, statistical analyses often assume that the influence

of meteorological variability on pollutant concentration can be cleanly separated from the influence of anthropogenic emissions changes. This is not completely possible, as the impacts of meteorological variability on pollutant concentration will also vary depending on the emissions. The degree to which this interaction affects the ability to calculate emissions-related trends under changing meteorology also remains unknown.

Here, we conduct a model experiment to evaluate the performance of widely-used statistical models in correcting for meteorological variability and estimating emissions-driven trends in air quality. We focus on the impacts of anthropogenic emissions changes on annual $PM_{2.5}$ and summer $O_3$ in the US (2011-2017) and China (2013-2017), two periods well-studied in previous literature. Using a 3-D atmospheric chemical transport model GEOS-Chem, we simulate two sets of scenarios – "observational scenarios" with assimilated meteorological inputs (with interannual variability) and "counterfactual scenarios" with constant meteorological inputs. Using simulated daily concentrations in the observational scenarios, we estimate meteorology-corrected trends for each grid cell using different statistical correction methods. We then compare the derived trends with the emissions-driven trends in the counterfactual scenarios (which are free of meteorological variability by design), calculating the resulting "error" in trend estimation. We further design a correction method based on GEOS-Chem constant emission simulations, and use it to quantify the degree to which attribution to meteorology and emissions separately is possible. Finally, we apply the different statistical correction methods to observational data from surface monitoring networks in the US and China, discussing the variability across different methods. We conclude by providing recommendations for techniques to evaluate air pollution policies under changing meteorological conditions.

## 2 Method

### 2.1 GEOS-Chem

GEOS-Chem is a global three-dimensional chemical transport model driven by assimilated meteorological data from the Goddard Earth Observation System (GEOS-5) of the NASA Global Modeling and Assimilation Office (GMAO) (Bey et al. (2001), http://www.geos-chem.org/). The simulation of $PM_{2.5}$ in GEOS-Chem represents an external mixture of secondary inorganic aerosols, carbonaceous aerosols, sea salt, and dust aerosols. GEOS-Chem includes detailed $O_3$-$NO_x$-volatile organic carbon (VOC)-aerosol-Halogen tropospheric chemistry (Travis et al., 2016; Sherwen et al., 2016). The GEOS-Chem model has been previously used to study the changes in $PM_{2.5}$ and $O_3$ during our studied periods, and model simulations have been shown to be consistent with the observed concentrations (e.g., see C. Li et al. (2017); Xie et al. (2019) for the US, and K. Li et al. (2018); Lu et al. (2019); Zhai et al. (2021) for China). Studies in both regions show that the GEOS-Chem model is able to reproduce the spatial, seasonal, and interannual variability and the long-term trends in observed pollutant concentrations, despite biases in absolute concentrations in certain species and regions (Heald et al., 2012; Travis et al., 2016; Tian et al., 2021).

We use GEOS-Chem version 12.3.0 with a horizontal resolution of $0.5^\circ \times 0.625^\circ$ in North America and Asia (Wang et al., 2004). For each scenario, we first conduct a global run at a horizontal resolution of $4^\circ \times 5^\circ$, with a 12 month spin-up. These global runs are then used as the boundary conditions for nested simulations in US and Asia with finer resolution of $0.5^\circ \times 0.625^\circ$.

### 2.2 GEOS-Chem scenarios

Table 1 shows the simulations included in our model experiments. We simulate two sets of scenarios – "observational scenarios" with interannual variability in meteorology and "counterfactual scenarios" with constant meteorological inputs. Both scenarios use

the same emissions inventory as input (see Method 2.3). For each grid cell, we estimate the linear trends in pollutant concentrations from simulated daily $PM_{2.5}$ and $O_3$ concentrations. We focus on the daily 24-hour average $PM_{2.5}$ of all seasons, and the maximum daily average 8-hour (MDA8) $O_3$ in summer (June, July, August). Our GEOS-Chem simulations use meteorological fields from the Modern-Era Retrospective analysis for Research and Applications, Version 2 (MERRA-2) (Gelaro et al., 2017). We aggregate the hourly meteorological data for consistency with the pollutant concentrations: a 24-hour average for $PM_{2.5}$ analysis and the corresponding 8-hour average for $O_3$. Meteorological features that are used in the statistical models can be found in 2.4.

#### *2.2.1 Observational scenarios*

Observational scenarios simulate $PM_{2.5}$ and $O_3$ under changing emissions and changing meteorological fields. Trends estimated under the observational scenarios ($\beta^{obs}$) are subject to the influences of interannual meteorological variability. Our model experiments were not specifically designed to reproduce observed air quality in these two regions, but rather to provide a realistic test case for our statistical experiments. Nevertheless, as shown in figure S1 and S2, the simulated concentrations in $PM_{2.5}$ and $O_3$ largely reproduce the daily variability in observed pollutant concentrations. The linear trends in simulated $PM_{2.5}$ and $O_3$ concentrations in the observational scenario are largely consistent with trends of the measured concentrations. For example, the average trend ($\pm$one standard deviation) in the US is -0.27$\pm$0.30 $\mu g^{-3}$/year (observation) and -0.39$\pm$0.24 ppb/year (GEOS-Chem) for $PM_{2.5}$, and -0.91$\pm$0.98 ppb/year (observation) and -1.02$\pm$0.83 ppb/year (GEOS-Chem) for $O_3$. The only exception is that our model cannot reproduce the increasing $PM_{2.5}$ trends in Northwest US because we do not consider the interannual variability in the biomass burning emissions.

#### *2.2.2 Counterfactual scenarios*

Counterfactual scenarios simulate $PM_{2.5}$ and $O_3$ under changing emissions but constant meteorology. All simulation years in the counterfactual scenario use the meteorological fields of the start year (2011 for US, 2013 for China). Trends estimated under the counterfactual scenario ($\beta^{count}$) are not subject to interannual meteorological variability; we use this as a proxy for the trends in pollutant concentrations driven by emissions changes alone.

It is important to note that we do not assume our GEOS-Chem simulations perfectly represent the underlying pollutant concentration in the real world (although the model compares relatively well with the observational data). Rather, our main focus is to evaluate how much different statistical methods can explain the differences between the observational and counterfactual scenarios. The assumption here is that the differences between observational and counterfactual scenarios are useful approximations of the impacts of meteorological variability on pollutant concentrations. The implications of uncertainty in GEOS-Chem for our results can be found in the discussion section.

| **GEOS-Chem scenarios** | **Emissions inventory** | **Meteorological fields** | **Trend estimates** | **Meteorological correction** |
|---|---|---|---|---|
| Counterfactual scenarios | **Changing** 2011-2017 (US) 2013-2017 (China) | **Constant** 2011 (US) 2013 (China) | $\beta^{count}$ | No correction needed |
| Observational scenarios | **Changing** 2011-2017 (US) 2013-2017 (China) | **Changing** 2011-2017 (US) 2013-2017 (China) | $\beta^{uncorrected}$ | No correction |
| | | | $\beta^{MLR}$ | Linear combination of local features |
| | | | $\beta^{GAM}$ | GAM using local features |
| | | | $\beta^{RF}$ | RF using local features |
| | | | $\beta^{LASSO-regional}$ | LASSO using local and regional features |
| | | | $\beta^{RF-regional}$ | RF using local and regional features |
| | | | $\beta^{gc}$ | Use simulations from constant emissions scenarios |
| Constant emissions scenarios | **Constant** 2011 (US) 2013 (China) | **Changing** 2011-2017 (US) 2013-2017 (China) | | |

Table 1: Overview of GEOS-Chem scenarios and meteorological correction methods.

### 2.3 Emissions inventory

For the US, we use the National Emissions Inventory 2011 (NEI 2011) as a baseline emissions inventory and scale the emissions in 2012 to 2017 to match the annual total emissions each year (U.S. Environmental Protection Agency, 2021b). For China, we use the monthly Multi-resolution Emission Inventory for China (MEIC) during 2013 to 2017 (M. Li et al., 2017; Zheng et al., 2018). During the studied time periods, US and China experienced dramatic decreases in anthropogenic emissions, particularly in $SO_2$ and $NO_x$. In the US, the total anthropogenic emissions of $SO_2$ decreased by 57% and $NO_x$ emissions decreased by 26% during 2011 to 2017 (see figure S3). In China, anthropogenic $SO_2$ emissions decreased by 59% and $NO_x$ emissions decreased by 21% during the 2013-2017 period (see figure S4).

Natural emissions of multiple chemical species are calculated online in the simulations (rather than prescribed) in the GEOS-Chem model and thus can be influenced by meteorological variability (see Keller et al. (2014) for more details). Impacts of meteorology on $PM_{2.5}$ and $O_3$ concentrations through changes in the natural emissions are

considered here as part of the meteorology - concentration relationship. These emissions include $NO_x$ emissions from lightning and soil processes, sea salt emissions, dust emissions, and biogenic volatile organic carbon (VOC) emissions. However, biomass burning emissions are prescribed in the GEOS-Chem model and we hold them constant at the level of the start year. We make this simplification because the GEOS-Chem model uses prescribed biomass burning emissions from external inventories such as Global Fire Emissions Database (Werf et al., 2017), and it is impossible to distinguish natural fire emissions (part of the meteorological variability) from anthropogenic fire emissions (e.g., from farm residual burning).

## 2.4 Statistical and machine learning models

### *2.4.1 Model with local meteorological variables*

We assess the performance of statistical and machine learning models to correct for the meteorological variability in the observational scenarios. We evaluate these methods with a commonly-used framework (e.g., used in K. Li et al. (2018) and Zhai et al. (2019)) which models the air pollutant concentrations of each individual grid cell using an additive form of a trend component, a meteorology component, and time fixed effects (to capture daily and monthly variability not related to meteorology). More specifically, we estimate the following regression equation for each grid cell $i$:

$$y_{it} = \beta_i^{obs} \times t + f_i(X_{it}) + \eta_{it} + \epsilon_{it} \tag{1}$$

where $y_{it}$ denotes the $PM_{2.5}$ or $O_3$ concentration at grid cell $i$ on day $t$. $t$ is the time index (e.g., in the US, $t$=1 for January 1st, 2011 and $t$=2 for January 2nd, 2011). $X_{it}$ denotes the local meteorology features (i.e. meteorological variables in grid cell $i$ on day $t$). $\eta_{it}$ is the month-of-year×day-of-month fixed effect to capture daily and monthly variability of pollutant concentrations that are not related to the meteorological variability (e.g., seasonal cycle in $O_3$ and $PM_{2.5}$). $\epsilon_{it}$ is the normally-distributed error term. $\beta_i^{obs}$ represents the meteorology-corrected trend in $PM_{2.5}$ or $O_3$ concentration for grid cell $i$ under a specific method. We use the absolute differences $|\beta_i^{obs} - \beta_i^{count}|$ to evaluate the performance of different methods to correct for meteorological variability for any given grid cell $i$.

Here, $f_i(X_{it})$ represents the specifications of local meteorological features for grid cell $i$ under different methods. In addition to the commonly-used multiple linear regression (MLR) model, we also evaluate following models with higher flexibility: polynomial regression models (quadratic, cubic), cubic spline models, generalized additive models (GAM, implemented with R package "mgcv" (Wood, 2011)), and Random Forest (RF) models. We focus on the methods in table 1 in the main manuscript, and the performance of the other methods can be found in table S1 and S2. Note that the time fixed effects are modelled differently in RF models due to the estimation procedure. More details on the implementation of RF can be found in SI.

We use the following ten variables from MERRA-2 as our selected meteorological features for the statistical analysis: surface temperature, precipitation, humidity, planetary boundary layer height, cloud fraction, surface air pressure, and wind speed (U and V direction, at surface and 850 hpa level). These variables are the most commonly used features in previous studies. We also perform sensitivity analyses that include nine more meteorological features: direct photosynthetically-active radiation, diffuse photosynthetically-active radiation, tropopause pressure, friction velocity, top soil moisture, root soil moisture, snow depth, surface albedo, and surface air density. These features are selected because they are used as primary or intermediate inputs for calculating $PM_{2.5}$ or $O_3$ concentrations in the GEOS-Chem model and may contain information that help explain variability in pollutant concentrations.

#### *2.4.2 Model with local and regional meteorological variables*

We also evaluate models that use both local and regional meteorological features. Regional meteorological features are important for explaining variability in local pollutant concentrations due to 1) pollution transport from neighboring locations, and 2) influences from meteorological systems at synoptic scale (i.e. large scale weather systems that span over 1000 kilometers such as circulation patterns) (Tai et al., 2012; Shen et al., 2015; H. Zhang et al., 2018; Leung et al., 2018; Han et al., 2020). As the incorporation of both local and regional features can quickly expand the dimensionality of the feature space, here we use the Least Absolute Shrinkage and Selection Operator (LASSO) and the Random Forest (RF) model, two statistical models that show good prediction performances with high dimensional data inputs. We estimate the following equations:

$$y_{it} = \beta_i^{obs} \times t + g_i(X_{it}, Z_t) + \eta_{it} + \epsilon_{it} \tag{2}$$

where $g_i()$ denotes the functional form fitted by LASSO or RF. $X_{it}$ again denotes the local meteorology features for grid cell $i$ on day $t$. $Z_t$ denotes the regional scale meteorology features including the meteorological features for every grid cell in the US on day $t$ (98 cells in 4×5 degrees; we choose a relatively coarse resolution due to computational cost). Meteorological information in each location in the US may help explain the pollutant concentrations in grid cell $i$. In total, we have 10 local features ($X_{it}$) and 10×98=980 regional scale features ($Z_t$). The coefficient $\beta_i^{obs}$ is obtained with the double machine learning approach by Chernozhukov et al. (2018). More details on the implementation of LASSO and RF can be found in SI.

### 2.5 Correction approach using GEOS-Chem constant emissions scenario

We further design and evaluate an approach to correct for meteorology variability with GEOS-Chem simulations (referred to as "constant-emis" approach). The "constant-emis" approach uses GEOS-Chem simulations with constant anthropogenic emissions and changing meteorological fields ("constant emissions scenarios" in table 1). All years in the constant emissions scenario use the anthropogenic emissions of the start year (2011 for US, 2013 for China). We estimate the following equations:

$$y_{it} = \beta_i^{gc} \times t + SIM_{it} + \eta_{it} + \epsilon_{it} \tag{3}$$

where $SIM_{it}$ denotes the simulated concentrations on day $t$ in grid cell $i$ in the constant emissions scenarios. $SIM_{it}$ serves a similar purpose as the term "$f_i(X_{it})$" in equation 1, but comes from the GEOS-Chem simulation. Some previous studies have also used model simulations with constant emissions input as a way to characterize meteorological variability (Zhong et al., 2018; Zhao et al., 2020). $\beta_i^{gc}$ is the estimated meteorology-corrected trend in $PM_{2.5}$ or $O_3$ concentration using this model-based correction method.

Compared to previous statistical and machine learning approaches, the "constant-emis" approach better captures the meteorological variability as simulated in GEOS-Chem (as $SIM_{it}$ are directly taken from GEOS-Chem). Therefore, the difference between the trend estimates ($\beta^{gc}$) and counterfactual trends ($\beta^{count}$) provides a conceptual lower bound for estimation errors using the framework of equation 1 to perform meteorological corrections. The commonly-used framework of equation 1 assumes that the impacts of meteorology variability can be separated from the impacts of anthropogenic emissions. In our experiments, this assumption indicates that the differences between the counterfactual scenario and the observational scenario can be solely explained by the meteorological variables. However, the difference in pollutant concentrations between these scenarios is also in part driven by emissions in their interaction with meteorology (despite the fact that our different scenarios use the same emissions inventory). We use $|\beta_i^{gc} - \beta_i^{count}|$ to quantify the estimation error associated with ignoring such interactions in this framework.

### 2.6 Air quality observation data

We use the surface air quality measurements from the Air Quality Systems administered by the US EPA (U.S. Environmental Protection Agency, 2021a). We use the daily 24-hour average of $PM_{2.5}$ concentrations for all months and the daily maximum 8-hour average (MDA8) $O_3$ concentrations for June, July and August. Figure S1 shows the locations, trends in measured concentrations, and correlations between GEOS-Chem simulations and measured concentrations.

The surface air quality measurements in China come from the monitoring network from China's Ministry of Ecology and Environment (China's Ministry of Ecology and Environment, 2021). The monitoring network was launched in 2013 and has expanded to all prefecture level cities in mainland China. We use the daily 24-hour average of $PM_{2.5}$ concentrations and the MDA8 $O_3$ concentrations for summer. Figure S2 shows the locations, trends in measured concentrations, and correlations between GEOS-Chem simulations and measured concentrations.

We use the meteorological variables from MERRA-2 when performing meteorology corrections at these monitoring stations, because the meteorology information is not available for all these variables at the station level. This is consistent with previous analysis estimating the meteorology-corrected trends of the observational air quality data (e.g., K. Li et al. (2018)).

## 3 Results

### 3.1 Performance of different correction methods: US (2011-2017)

Figure 1A and 1C show the trends in $PM_{2.5}$ and $O_3$ concentrations in the counterfactual scenarios in the US. When holding meteorological fields constant across years, decreasing trends in the simulated $PM_{2.5}$ concentrations across the US result from decreasing anthropogenic emissions. In particular, the counterfactual scenario has substantial declining trends in $PM_{2.5}$ in the East US where $SO_2$ emissions decreased dramatically. The scenario also has negative linear trends in $O_3$ concentrations in all but three grid cells in the West. Increases in summer $O_3$ in these locations result from the nonlinear relationship between $O_3$ concentrations and $NO_x$ emissions.

Figure 1B shows the degree to which different meteorological correction methods can recover the emissions-driven trends in the counterfactual scenarios. The figure shows the magnitude of estimation error in trend estimates in $PM_{2.5}$ for each grid box ($|\beta^{obs} - \beta^{count}|$). When no correction for meteorology is performed ("uncorrected" in figure 1B), we observe large estimation errors in trend estimates over the Northeast and Southern US by up to 0.25 $\mu$g m$^{-3}$/year, an error that is 50% of the trend estimates under the counterfactual scenarios. We find that the widely-used MLR method does not help reduce these errors in $PM_{2.5}$ trend attribution. MLR has a modest impact on reducing the errors in Northeast US, but it does not decrease the errors over the Southern US and leads to higher errors over Midwest. Nationwide, the average magnitude of errors (relative to the counterfactual scenario) slightly increases with the MLR correction (0.083 $\mu$g m$^{-3}$/year) compared to the uncorrected case (0.066 $\mu$g m$^{-3}$/year). Among the five methods, we find that the RF model using both local and regional scale features ("RF-regional" in figure 1) offers the best performance in recovering the trends in the counterfactual scenarios and is the only method that yields smaller errors than the uncorrected case (the nationwide average error decreased by 0.019 $\mu$g m$^{-3}$/year, or 28% less). The RF-regional model also outperforms the RF-local and LASSO-regional models, suggesting the importance of considering non-linearity, interactions between different meteorological features, and regional meteorology information in correctly adjusting for the impacts of meteorology.

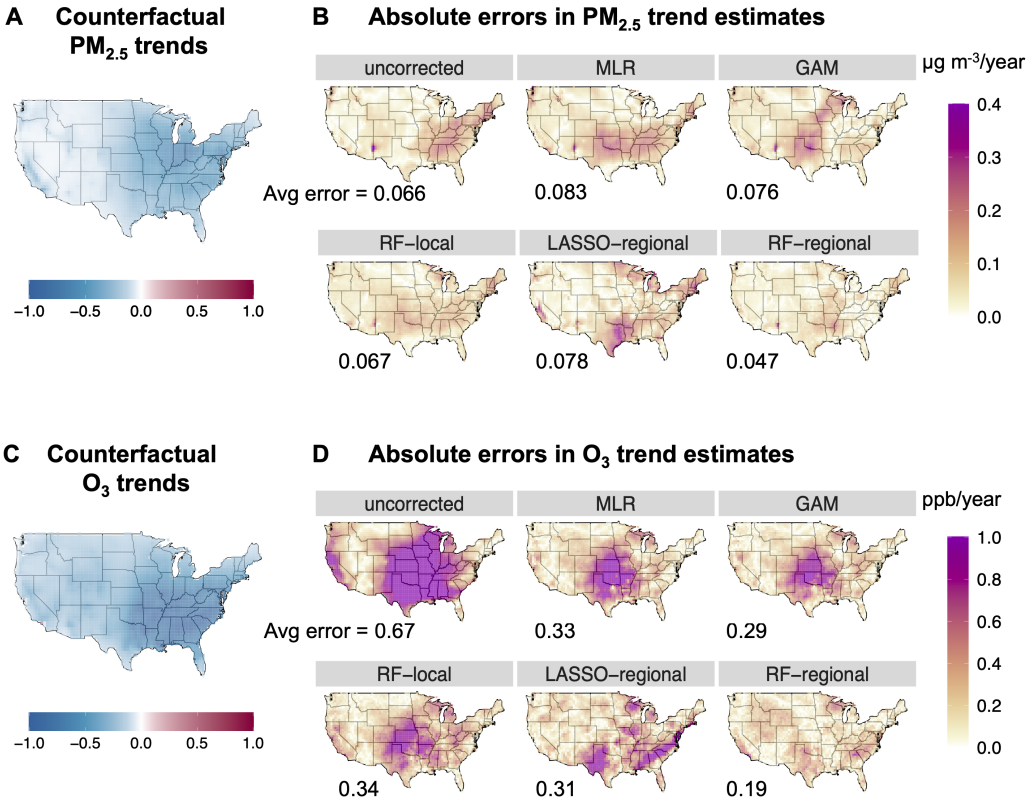


Figure 1: Trend estimates of daily annual $PM_{2.5}$ (Panels A and B) and summer $O_3$ (C and D) in the US. Panels A and C show trend estimates under the counterfactual scenario ($\beta^{count}$). Panels B and D show the absolute magnitude of errors of trend estimates under different correction methods compared with the counterfactual scenarios ($|\beta^{obs} - \beta^{count}|$). The average of the absolute errors for each method is shown in the figure. Unit of trend estimate is $\mu$g $m^{-3}$/year for $PM_{2.5}$ or ppb/year for $O_3$.

Meteorological variability has a substantial influence on the summertime $O_3$ trends in the US during this period (as shown in figure 1D). Relative to the counterfactual scenario, the uncorrected $O_3$ trends are biased by over 1-2 ppb/year in large areas of California, Midwest and Southern US (as much as 320% of the counterfactual trends). This is largely driven by the fact that the 2011 and 2012 summer was particularly hot in these regions and led to higher concentrations of $O_3$ at the beginning of this 7-year period (see figure S6 for the Southern and Midwest US). Therefore, failure to correct for meteorological variability results in much more negative trend estimates in the $O_3$ concentrations in these areas compared to the counterfactual scenario (see figure S5). Meteorology corrections with MLR or GAM help reduce these estimation errors substantially (nationwide average error is reduced by 51% using MLR or 57% using GAM compared to uncorrected trends), while large errors still persist in the Midwest and South. Similar to the case of $PM_{2.5}$, the RF-regional model offers the best performance in correcting for meteorological variability (the national average error is further reduced by 42%, compared to MLR), and it is especially helpful in reducing the errors over the Midwest and South (regional average error is reduced by 64% and 44%, respectively, compared to MLR).

### 3.2 Performance of different correction methods: China (2013-2017)

Figure 2A and 2C show the trends in $PM_{2.5}$ and $O_3$ concentrations in the counterfactual scenarios in China. We find a substantial decline in simulated $PM_{2.5}$ concentration during 2013 to 2017, particularly in eastern and central China. In contrast, there is little change in the simulated $PM_{2.5}$ concentrations in western China in the counterfactual scenario, where $PM_{2.5}$ is dominated by dust species largely driven by natural processes (see figure S8). For summer $O_3$, there are decreasing trends in the counterfactual scenario in most parts of China, except for North China and some urban areas. This is largely consistent with previous studies that attempt to attribute emissions-related changes in $O_3$ concentrations during this period based on modeling or observational data (K. Li et al., 2018, 2020; Lu et al., 2020).

Figure 2B shows the magnitude of estimation errors in the trend estimates of annual $PM_{2.5}$ in China under different correction methods. We find the underlying meteorological variability has a substantial impact on $PM_{2.5}$ trends in China during this period. We observe large differences between the uncorrected and counterfactual trends in simulated $PM_{2.5}$ concentrations, particularly in Northwest and Northeast China. Similar to the model experiments in the US, we find that MLR and GAM methods fail to correct for this underlying meteorological variability and lead to further increases in estimation errors in many locations. Relative to the counterfactual scenario, the nationwide average error increases to 0.90 $\mu$g m$^{-3}$/year with MLR and 1.06 $\mu$g m$^{-3}$/year with GAM (compared to 0.89 $\mu$g m$^{-3}$/year with no correction). We find that the RF-regional model recovers the counterfactual trends better than other methods (nationwide average error: 0.64 $\mu$g m$^{-3}$/year; an improvement by 30% relative to MLR), but it is still not able to correct for the persistent estimation errors over Northwest China. We further analyze the performance of correction methods for the different component species of $PM_{2.5}$. As shown in figure S9 and S10, the MLR model is particularly unable to correct for the impacts of meteorological variability on nitrate and dust species. Compared with MLR, the RF-regional model better corrects for the impacts of meteorology on secondary organic aerosol species in South and Central China and ammonium in Northeast, but only yields modest improvement in correcting for the errors in dust concentrations over Northwest China (see figure S11). In a sensitivity analysis, we use an approach that first fits RF-regional models of each individual $PM_{2.5}$ species, and then combine predictions to each species to derive trend estimates. The results are largely similar to the main approach that fits models to the total $PM_{2.5}$ concentration (see figure S12).

Figure 2D shows the magnitude of errors in the trend estimates for summer $O_3$ under different correction methods in China. We find that the MLR model only modestly

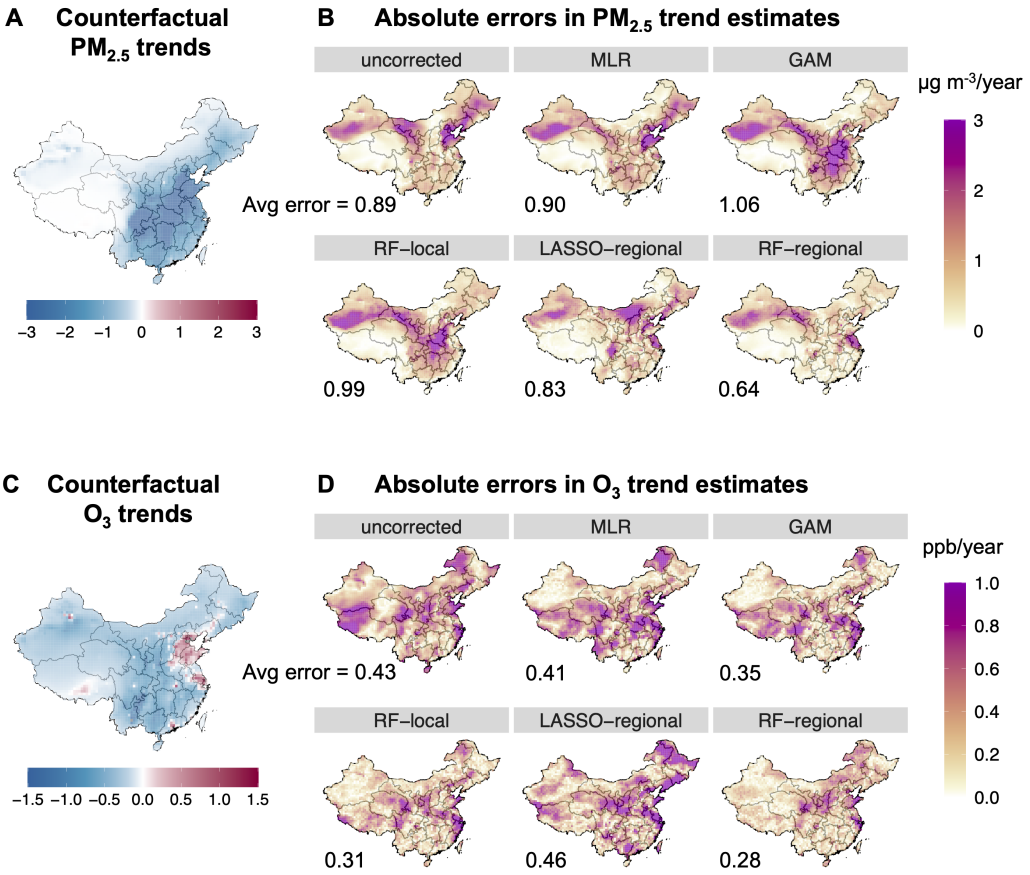


Figure 2: Trend estimates of daily annual $PM_{2.5}$ (Panels A and B) and summer $O_3$ (C and D) in China. Panels A and C show trend estimates under the counterfactual scenario ($\beta^{count}$). Panels B and D show the absolute magnitude of errors of trend estimates under different correction methods compared with the counterfactual scenarios ($|\beta^{obs} - \beta^{count}|$). The average of the absolute errors for each method is shown in the figure. The unit of the trend estimate is $\mu$g $m^{-3}$/year for $PM_{2.5}$ or ppb/year for $O_3$.

reduces the estimation errors compared to the uncorrected cases, and the RF-regional model offers the best overall performance. The nationwide average error is reduced to 0.28 ppb/year using the RF-regional model (relative to 0.43 ppb/year uncorrected and 0.41 ppb/year with MLR). Similar to the evaluation of summer time $O_3$ in the US, we find the non-linear models (GAM, RF-local) perform better than MLR, but are not as good as the RF-regional model. Surprisingly, the LASSO-regional model performs the worst in recovering the counterfactual trends. This suggests the importance of considering non-linearity and regional meteorological features in understanding the $O_3$ – meteorology relationships. Compared to the US case, we find the impacts of meteorological variability on $O_3$ and the method performances are much more spatially heterogeneous (see figure S5, S7), which may be partially due to the more heterogeneous $O_3$ regimes in China during this period.

### 3.3 Limitations in separating meteorological and emissions influence: quantified with constant emission scenarios

In our model experiments in both US and China, we find large differences remain between the trends evaluated with statistical models (even the best-performed RF-regional model) and counterfactual trends. The remaining differences could result from two different factors: 1) the statistical model cannot capture the complex relationship between meteorology and pollutant concentrations, and/or 2) the differences between the observational scenarios and counterfactual scenarios depend not only on the meteorological variability but also the anthropogenic emissions in their interaction with meteorology (i.e. impacts of meteorology on air quality also depends on the level of emissions).

We quantify the potential magnitude of this second factor using our constant-emis approach. As the constant-emis approach captures the exact relationship between meteorology and pollutant concentrations in GEOS-Chem, the error of the constant-emis approach is only associated with the second factor above and thus provides a conceptual lower bound of the estimation errors that can be achievable by any statistical approaches. Figure 3 shows the estimation errors of trend estimates using the constant emissions scenarios simulated by GEOS-Chem. We focus on the trends in summer $O_3$ in the US and annual $PM_{2.5}$ in China, for which we see the largest impacts of meteorological variability on the pollutant trends and the largest improvements in reducing estimation errors from the correction methods. Compared to the statistical models (e.g., MLR and RF-regional in figure 3A and 3C), trends evaluated using the constant-emis approach are very similar to the trends in the counterfactual scenarios. The national average error of trend estimates is only 0.04 ppb/year for the $O_3$ trends in the US (relative to 0.33 ppb/year under MLR or 0.19 ppb/year under RF-regional), and only 0.08 $\mu$g m$^{-3}$/year for the $PM_{2.5}$ trends in China (relative to 0.91 $\mu$g m$^{-3}$/year under MLR or 0.64 $\mu$g m$^{-3}$/year under RF-regional).

However, the estimation errors calculated above are non-negligible and can be large in certain regions. As shown in Figure 3B and 3D, the constant-emis approach generally yields trend estimates biased by 10% relative to the counterfactual trends, but the errors can be up to 40% in certain areas. This error term is the result of ignoring how emissions could potentially influence the impacts of meteorology on the pollutant concentrations – that is, the impacts of the same meteorological variability on concentrations may be different in the start year (with high emissions) compared to the end year (with low emissions).

### 3.4 Application to observational data

Figure 4 shows the regional trends in $O_3$ in the US and trends in $PM_{2.5}$ in China estimated from the GEOS-Chem simulations and the measured concentrations from surface monitoring networks (only grid cells that overlap with monitor locations are shown

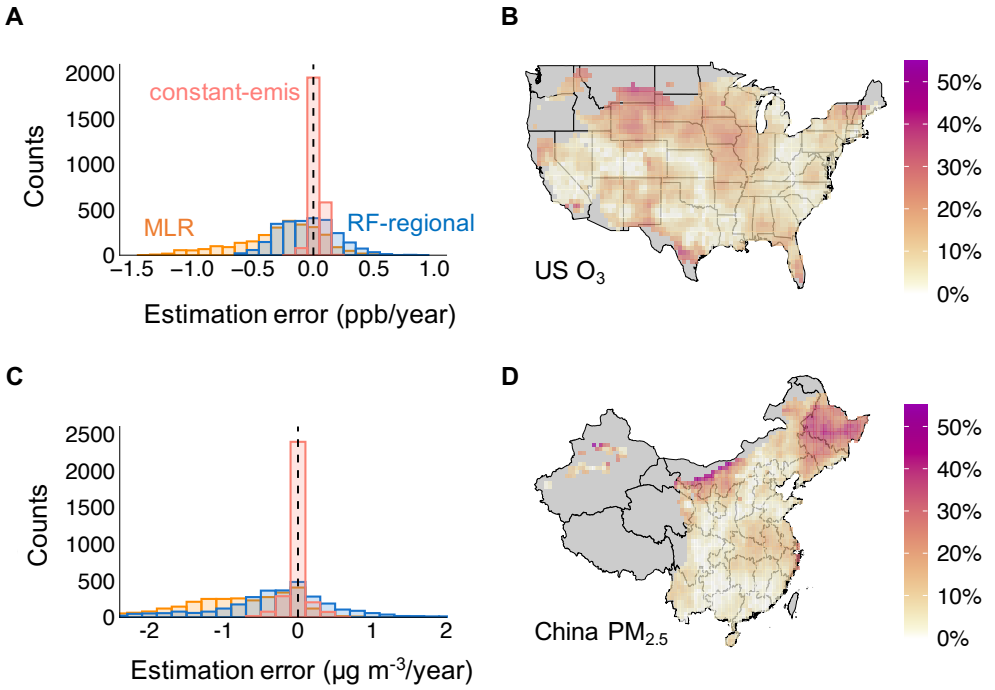


Figure 3: Panels A and C show the histogram of estimation errors in trend estimates assessed using MLR, RF-regional and constant-emis. Panels B and D show the percentage of the errors assessed with the constant-emis method relative to the trends in the counterfactual scenario ($|\beta^{gc} - \beta^{count}|/|\beta^{count}|$). Panels B and D only show grid cells with a trend in the counterfactual scenarios >0.2 ppb/year or >0.2 $\mu$g $m^{-3}$/year; remaining grid cells are shown in gray. Panels A and B illustrate the summer $O_3$ trends in the US. Panels C and D illustrate the annual $PM_{2.5}$ trends in China.

here). As shown in figure 4A, how to correct for meteorological variability is important for attributing summer $O_3$ trends to emissions reductions in the US. Based on measured concentrations, the regional average uncorrected $O_3$ trend is -1.49 ppb/year and -1.15 ppb/year in Midwest and Southern US, respectively, which overestimates the reductions in concentrations attributable to anthropogenic emissions changes. Correcting for the meteorological variability with MLR model yields regional average trend at -0.54 ppb/year in Midwest (a decrease by 53% in magnitude relative to uncorrected trends) and -0.71 ppb/year in the Southern US (a decrease by 52%). RF-regional model further reduces the absolute magnitude of the declines in $O_3$ attributable to emissions reductions to -0.02 ppb/year for Midwest and -0.40 ppb/year for the Southern US. Importantly, these patterns are consistent with the results from our model experiments in these regions. For example in the GEOS-Chem simulation, the RF-regional model also estimates a much less negative emissions-driven trend in the Southern US compared to the uncorrected case and MLR estimates. For the GEOS-Chem simulations, RF-regional estimates are 39% smaller than MLR estimates, and this is comparable to the magnitude changes for the observational data (RF-regional estimates are 44% smaller than MLR). As the RF-regional model performs the best in recovering counterfactual trends in the GEOS-Chem simulations, this suggests RF-regional may also perform the best in recovering the underlying emission-driven trends when applying to the observational data.

Figure 4B shows the trends in $PM_{2.5}$ concentrations estimated from the GEOS-Chem simulation and the observational data from China's surface monitoring network using different correction methods. Based on the observational data, our analysis reveals that the choice of methods for meteorological correction can yield very different results for certain regions. Much smaller reduction of $PM_{2.5}$ concentrations is attributed to anthropogenic emissions changes in the North, Northeast and East of China using the RF-regional model, relative to the MLR estimates. For example, the average emissions-driven trend estimated from the observational data is -4.9 $\mu$g m$^{-3}$/year in Beijing under the RF-regional model, compared with -9.6 $\mu$g m$^{-3}$/year under the MLR model. These patterns are consistent with the patterns of the trend estimates estimated from our GEOS-Chem simulations with different statistical methods.

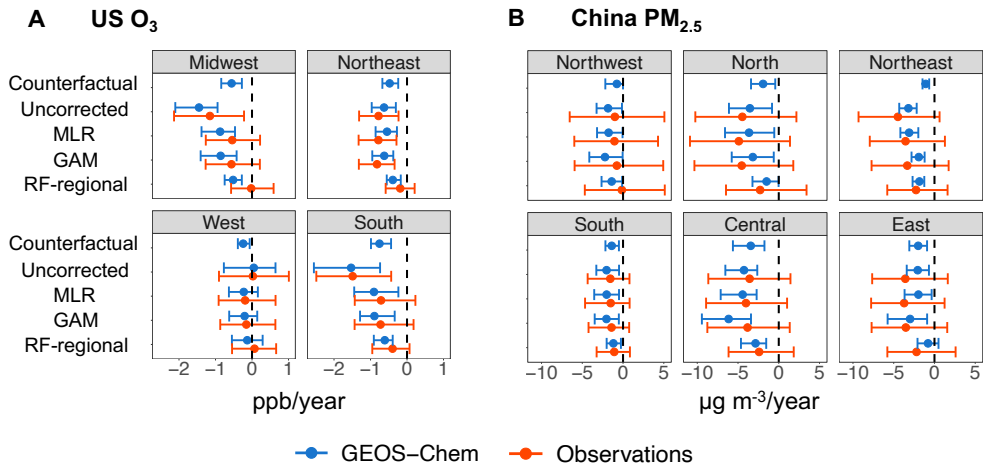


Figure 4: Trends in $O_3$ in the US (panel A) and $PM_{2.5}$ in China (panel B) estimated from the observational data (red) and GEOS-Chem simulations (blue) under different correction methods. Trends in pollutant concentrations are estimated at the monitor level (for the observational data) or at the grid cell level (for GEOS-Chem simulations). The point indicates the average value of the assessed trends of all monitors (or grid cells) within a region. The error bars show the 10th and 90th percentile of the assessed trends of all monitors/grid cells within a region. Panel A illustrates the summer $O_3$ trends in the US (unit: ppb/year). Panel B illustrates the annual $PM_{2.5}$ trends in China (unit: $\mu$g/m$^3$/year). We classify the US states into four regions according to the US Census Bureau and classify China's provinces into six regions based on the structure of China's subnational electric grid.

## 4 Discussion

We designed a model experiment that enables us to directly quantify the performance of different statistical models to evaluate the causal trends in pollutant concentrations driven by anthropogenic emissions changes. Based on our evaluations of either $PM_{2.5}$ or $O_3$ trends across US and China during periods of recent emission declines, our analysis shows that widely-used MLR and GAM methods do not perform well in correcting for the meteorological variability and recovering simulated emissions-driven trends. We propose a random forest model that uses both local and regional meteorological features, which offers the best overall performance in recovering the emissions-driven trends across both species and countries. Applying this model to observational data suggests that estimates based on MLR or similar methods may overestimate the impacts of an-

thropogenic emissions changes on the decline of pollutant concentrations in certain regions in the US and China. However, the RF-regional method does not outperform all the other approaches in every location despite its better overall performance (see figures S13 and S14). This suggests that using multiple statistical approaches may be necessary to derive robust conclusions for attributing pollutant trends to emission changes.

With our model experiments, we also quantify the estimation errors in assuming the emission impacts can be perfectly separated from the meteorological variability. These errors likely bound the estimation errors that can be achieved by any statistical corrections of meteorological variability with this assumption. In the future, more complex statistical and machine learning methods could be applied to distinguish emissions- and meteorologically-driven changes, but attribution solely based on observed concentrations and meteorology will be limited by physical interactions between emissions and meteorology. We find that the estimation errors resulting from these interactions are overall much smaller compared to the estimation errors of the existing statistical methods, but can still be important for certain regions at certain times. Furthermore, the intertwined relationships between emissions and meteorology are also much more complex in reality compared to our model experiments. For example, meteorology can also directly influence anthropogenic emissions (e.g., increased electricity consumption during extreme weather conditions (U.S. Energy Information Agency, 2019; He et al., 2020)). Therefore, the estimation errors that can be achieved by more flexible statistical models can potentially be even bigger than the errors quantified with our constant-emis approach.

While the GEOS-Chem model provides us with a framework for causal experiments to test statistical methods, its use in our model experiments introduces some uncertainty and limitations. Specifically, our experiments assess the performance of statistical methods in correcting for the meteorology-pollution relationships encoded in GEOS-Chem, which may differ from the complex relationships observed in the observational data. Several studies have shown that GEOS-Chem and similar models do not capture certain meteorology-pollution relationships in the observational data (e.g., temperature - $O_3$ relationship (Porter & Heald, 2019) and influence of regional meteorological patterns (Fiore et al., 2009)). The relationships encoded in GEOS-Chem may be different from the underlying meteorology-pollution relationships in the following three ways: (1) parameters in GEOS-Chem that describe these relationships are uncertain; (2) the relationships in GEOS-Chem are incorrect or incomplete; and (3) the relationships in GEOS-Chem are deterministic compared to the potential stochastic underlying processes. While the parameterization schemes of the model may have little impact on our assessment of the statistical methods if the functional forms are correct, different functional forms may affect the relative performance of various statistical methods. The performance of any individual statistical method is likely to be worse in the real world compared to its ability to reproduce a deterministic meteorology-pollution relationship encoded in GEOS-Chem. Further model-based experiments could apply our methods to different atmospheric models in order to test if these conclusions differ by different models.

Our research reveals multiple directions for future research to enhance our understanding of the usage of statistical models to evaluate trends in pollutant concentrations under changing meteorological conditions. One key but challenging question is to better understand the estimation errors of these existing approaches, e.g. why the MLR model is able to correct for the meteorological variability in some locations but not others. In this paper, we only test a selection of methods based on their popularity in the existing literature and propose a simple-to-use model (RF-regional). More complex models (such as convolutional neural networks) may offer better performance, but the estimation error will likely be bounded by the errors of the constant-emis approach. Our work only evaluates the statistical and machine learning models in expressions 1 and 2, which only represent one (popular) set of evaluations that performs location-specific trend estimation with adjustments for meteorology and secular trends. However, other statis-

tical model specifications specifically targeted to questions of meteorological interaction or that permit borrowing information across locations may generate different results. A deeper investigation of the estimation error due to assuming perfect separation between meteorology and emission is also essential for understanding how we should interpret studies that use these statistical methods. For example, further work could explore how these errors will vary by the magnitude of emissions reductions and the chemistry regimes. Our analysis suggests the relative performance of different methods is largely similar in monitoring data and the GEOS-Chem experiments (at least for certain regions). It is interesting to further explore how the patterns of performance might differ across different types of monitor locations and conditions.

## 5 Recommendations for attributing trends to emissions changes

Using statistical methods to causally infer relationships between simulated air pollutant concentrations and anthropogenic emissions is challenging, not to mention understanding the drivers of observed air pollutants in the real world. Understanding the uncertainty of statistical models in characterizing the meteorology-pollution relationship is essential to evaluating the effectiveness of policy interventions with observational data. Here, we make several recommendations to researchers and policy makers based on our analysis.

For those who aim to infer causal effects of emissions changes on air quality based on observational data on concentrations and meteorology, we recommend using multiple statistical methods to correct for the meteorological variability when evaluating the impacts of policies or interventions on air quality. From our two case studies, we find a relatively large variability between the trend parameters estimated by different statistical methods (especially at the grid cell or monitor level). Some methods perform better in certain locations but not in others (though RF-regional is the best-performing method overall). Using multiple approaches (linear/non-linear and at local/regional scale) may help to quantify uncertainty related to meteorology corrections. These findings also suggest that empirical analyses may benefit from considering the impacts of meteorological variability on air quality separately for each region or even for each monitor location (if data permits), instead of attempting to determine a general relationship between meteorological variability and air pollution over a large spatial domain. Finally, analysts should be particularly cautious when using statistical methods to estimate impacts of anthropogenic emissions on air quality in regions where pollution variability is dominated by meteorologically-influenced environmental processes such as dust emissions, as we consistently show that typical statistical methods (in combination with the standard set of meteorological variables) do not work well in those regions.

Due to the non-negligible estimation errors in recovering the counterfactual trends even with the best-performed statistical approach we test, we believe these statistical analyses are most useful in understanding the patterns of anthropogenic emissions on air quality when aggregated across larger spatial areas, rather than providing specific trends for individual monitor locations. There is a higher degree of consistency among the trend estimates across different methods when aggregated at regional level, but assessment at local level is more sensitive to method choices. The absolute magnitude of monitor-level trends need to be interpreted with caution, considering both the uncertainty from the statistical methods and also the limit of meteorological correction due to ignoring the interactions between meteorology and emissions.

Because measured pollutant concentrations are subject to the influence of underlying meteorological variability, many efforts have attempted to correct for the impacts of meteorological variability and use "meteorology-corrected" concentrations and trends to assist in evaluating the effectiveness of air quality policies. Our study evaluates existing methods that aim to correct for the meteorological variability and finds many of

these methods do not perform well. This raises potential concerns about the use of "meteorology-corrected" concentrations as targets for policy evaluation. Meteorology-corrected concentrations and trends remain useful metrics to quantify the influence of emissions. However, a more comprehensive evaluation of the effectiveness of policy requires interpreting measurements with all available tools, ideally including both statistical analyses and physical models.

**Acknowledgments**

We thank Colette Heald and Valerie Karplus for helpful comments and discussions. We thank Yixuan Zheng for assistance with the MEIC emissions inventory. We thank Ke Li for sharing code of step-wise MLR analysis. This publication was supported by US EPA grant RD-835872-01. Its contents are solely the responsibility of the grantee and do not necessarily represent the official views of the USEPA. Further, USEPA does not endorse the purchase of any commercial products or services mentioned in the publication.

The GEOS-Chem simulation of different scenarios, code for different statistical methods and monitor-level trend estimates will be made available to readers in a public repository.

## References

Beijing Municipal Ecology and Environment Bureau. (2013). Beijing clean air action plan (2013–2017). , *744*, 140837. Retrieved from `http://sthjj.beijing.gov.cn/bjhrb/index/xxgk69/sthjlyzwg/wrygl/603133/index.html`

Bey, I., Jacob, D. J., Yantosca, R. M., Logan, J. A., Field, B. D., Fiore, A. M., ... Schultz, M. G. (2001). Global modeling of tropospheric chemistry with assimilated meteorology: Model description and evaluation. *Journal of Geophysical Research Atmospheres*, *106*(D19), 23073–23095. doi: 10.1029/2001JD000807

Camalier, L., Cox, W., & Dolwick, P. (2007). The effects of meteorology on ozone in urban areas and their use in assessing ozone trends. *Atmospheric Environment*, *41*(33), 7127–7137. doi: 10.1016/j.atmosenv.2007.04.061

Carslaw, D. C., Beevers, S. D., & Tate, J. E. (2007). Modelling and assessing trends in traffic-related emissions using a generalised additive modelling approach. *Atmospheric Environment*, *41*(26), 5289–5299. doi: 10.1016/j.atmosenv.2007.02.032

Chen, L., Zhu, J., Liao, H., Yang, Y., & Yue, X. (2020). Meteorological influences on pm2. 5 and o3 trends and associated health burden since china's clean air actions. *Science of The Total Environment*, *744*, 140837.

Chen, Z., Chen, D., Kwan, M. P., Chen, B., Gao, B., Zhuang, Y., ... Xu, B. (2019). The control of anthropogenic emissions contributed to 80% of the decrease in PM2.5 concentrations in Beijing from 2013 to 2017. *Atmospheric Chemistry and Physics*, *19*(21), 13519–13533. doi: 10.5194/acp-19-13519-2019

Cheng, J., Su, J., Cui, T., Li, X., Dong, X., Sun, F., ... He, K. (2019). Dominant role of emission reduction in PM2.5 air quality improvement in Beijing during 2013-2017: A model-based decomposition analysis. *Atmospheric Chemistry and Physics*, *19*(9), 6125–6146. doi: 10.5194/acp-19-6125-2019

Chernozhukov, V., Chetverikov, D., Demirer, M., Duflo, E., Hansen, C., Newey, W., & Robins, J. (2018). *Double/debiased machine learning for treatment and structural parameters.* Oxford University Press Oxford, UK.

China's Ministry of Ecology and Environment. (2021). *National Air Quality Monitoring Data.* Retrieved from `https://quotsoft.net/air/`

European Union. (2020). Air quality standards in the european union. , *744*, 140837. Retrieved from `https://ec.europa.eu/environment/air/quality/standards.htm`

Fiore, A. M., Dentener, F., Wild, O., Cuvelier, C., Schultz, M., Hess, P., ... others (2009). Multimodel estimates of intercontinental source-receptor relationships for ozone pollution. *Journal of Geophysical Research: Atmospheres*, *114*(D4).

Gelaro, R., McCarty, W., Suárez, M. J., Todling, R., Molod, A., Takacs, L., ... others (2017). The modern-era retrospective analysis for research and applications, version 2 (merra-2). *Journal of climate*, *30*(14), 5419–5454.

Grange, S. K., Carslaw, D. C., Lewis, A. C., Boleti, E., & Hueglin, C. (2018). Random forest meteorological normalisation models for Swiss PM10 trend analysis. *Atmospheric Chemistry and Physics*, *18*(9), 6223–6239. doi: 10.5194/acp-18-6223-2018

Han, H., Liu, J., Shu, L., Wang, T., & Yuan, H. (2020). Local and synoptic meteorological influences on daily variability in summertime surface ozone in eastern China. *Atmospheric Chemistry and Physics*, *20*(1), 203–222. doi: 10.5194/acp-20-203-2020

Hayn, M., Beirle, S., Hamprecht, F. A., Platt, U., Menze, B. H., & Wagner, T. (2009). Analysing spatio-temporal patterns of the global NO2- distribution retrieved from GOME satellite observations using a generalized additive model. *Atmospheric Chemistry and Physics*, *9*(17), 6459–6477. doi: 10.5194/acp-9-6459-2009

He, P., Liang, J., Qiu, Y. L., Li, Q., & Xing, B. (2020). Increase in domestic electricity consumption from particulate air pollution. *Nature Energy*, *5*(12), 985–995.

Heald, C. L., Collett, J. L., Lee, T., Benedict, K. B., Schwandner, F. M., Li, Y., ... Pye, H. O. (2012). Atmospheric ammonia and particulate inorganic nitrogen over the United States. *Atmospheric Chemistry and Physics*, *12*(21), 10295–10312. doi: 10.5194/acp-12-10295-2012

Henneman, L. R., Holmes, H. A., Mulholland, J. A., & Russell, A. G. (2015). Meteorological detrending of primary and secondary pollutant concentrations: Method application and evaluation using long-term (2000-2012) data in Atlanta. *Atmospheric Environment*, *119*, 201–210. doi: 10.1016/j.atmosenv.2015.08.007

Holland, D. M., Principe, P. P., & Sickles, J. E. (1998). Trends in atmospheric sulfur and nitrogen species in the eastern United States for 1989-1995. *Atmospheric Environment*, *33*(1), 37–49. doi: 10.1016/S1352-2310(98)00123-X

Keller, C. A., Long, M. S., Yantosca, R. M., Da Silva, A., Pawson, S., & Jacob, D. J. (2014). Hemco v1. 0: a versatile, esmf-compliant component for calculating emissions in atmospheric models. *Geoscientific Model Development*, *7*(4), 1409–1417.

Leung, D. M., Tai, A. P., Mickley, L. J., Moch, J. M., Van Donkelaar, A., Shen, L., & Martin, R. V. (2018). Synoptic meteorological modes of variability for fine particulate matter (PM2.5) air quality in major metropolitan regions of China. *Atmospheric Chemistry and Physics*, *18*(9), 6733–6748. doi: 10.5194/acp-18-6733-2018

Li, C., Martin, R. V., Van Donkelaar, A., Boys, B. L., Hammer, M. S., Xu, J. W., ... Zhang, Q. (2017). Trends in Chemical Composition of Global and Regional Population-Weighted Fine Particulate Matter Estimated for 25 Years. *Environmental Science and Technology*, *51*(19), 11185–11195. doi: 10.1021/acs.est.7b02530

Li, K., Jacob, D. J., Liao, H., Shen, L., Zhang, Q., & Bates, K. H. (2018, dec). Anthropogenic drivers of 2013-2017 trends in summer surface ozone in China. *Proceedings of the National Academy of Sciences of the United States of America*, *116*(2), 422–427. Retrieved from `http://www.ncbi.nlm.nih.gov/pubmed/30598435` doi: 10.1073/pnas.1812168116

Li, K., Jacob, D. J., Shen, L., Lu, X., De Smedt, I., & Liao, H. (2020). Increases in surface ozone pollution in china from 2013 to 2019: anthropogenic and

meteorological influences. *Atmospheric Chemistry and Physics*, *20*(19), 11423–11433.

Li, M., Liu, H., Geng, G., Hong, C., Liu, F., Song, Y., ... He, K. (2017). Anthropogenic emission inventories in China: A review. *National Science Review*, *4*(6), 834–866. doi: 10.1093/nsr/nwx150

Lu, X., Zhang, L., Chen, Y., Zhou, M., Zheng, B., Li, K., ... Zhang, Q. (2019). Exploring 2016-2017 surface ozone pollution over China: Source contributions and meteorological influences. *Atmospheric Chemistry and Physics*, *19*(12), 8339–8361. doi: 10.5194/acp-19-8339-2019

Lu, X., Zhang, L., Wang, X., Gao, M., Li, K., Zhang, Y., ... Zhang, Y. (2020). Rapid increases in warm-season surface ozone and resulting health impact in china since 2013. *Environmental Science & Technology Letters*, *7*(4), 240–247.

Ma, Z., Xu, J., Quan, W., Zhang, Z., Lin, W., & Xu, X. (2016). Significant increase of surface ozone at a rural site, north of eastern China. *Atmospheric Chemistry and Physics*, *16*(6), 3969–3977. doi: 10.5194/acp-16-3969-2016

McClure, C. D., & Jaffe, D. A. (2018). US particulate matter air quality improves except in wildfire-prone areas. *Proceedings of the National Academy of Sciences of the United States of America*, *115*(31), 7901–7906. doi: 10.1073/pnas.1804353115

Otero, N., Sillmann, J., Mar, K. A., Rust, H. W., Solberg, S., Andersson, C., ... Butler, T. (2018). A multi-model comparison of meteorological drivers of surface ozone over Europe. *Atmospheric Chemistry and Physics*, *18*(16), 12269–12288. doi: 10.5194/acp-18-12269-2018

Porter, W. C., & Heald, C. L. (2019). The mechanisms and meteorological drivers of the ozone–temperature relationship. *Atmospheric Chemistry and Physics Discussions*(x), 1–26. doi: 10.5194/acp-2019-140

Qu, L., Liu, S., Ma, L., Zhang, Z., Du, J., Zhou, Y., & Meng, F. (2020). Evaluating the meteorological normalized PM2.5 trend (2014–2019) in the "2+26" region of China using an ensemble learning technique. *Environmental Pollution*, *266*, 115346. Retrieved from `https://doi.org/10.1016/j.envpol.2020.115346` doi: 10.1016/j.envpol.2020.115346

Runge, J., Bathiany, S., Bollt, E., Camps-Valls, G., Coumou, D., Deyle, E., ... Zscheischler, J. (2019). Inferring causation from time series in Earth system sciences. *Nature Communications*, *10*(1), 1–13. Retrieved from `http://dx.doi.org/10.1038/s41467-019-10105-3` doi: 10.1038/s41467-019-10105-3

Saari, R., Mei, Y., Monier, E., & Garcia-Menendez, F. (2019). Effect of health-related uncertainty and natural variability on health impacts and co-benefits of climate policy. *Environmental Science and Technology*, *53*(3), 1098–1108. doi: 10.1021/acs.est.8b05094

Shen, L., Mickley, L. J., & Tai, A. P. (2015). Influence of synoptic patterns on surface ozone variability over the eastern United States from 1980 to 2012. *Atmospheric Chemistry and Physics*, *15*(19), 10925–10938. doi: 10.5194/acp-15-10925-2015

Sherwen, T., Schmidt, J. A., Evans, M. J., Carpenter, L. J., Großmann, K., Eastham, S. D., ... Ordóñez, C. (2016). Global impacts of tropospheric halogens (Cl, Br, I) on oxidants and composition in GEOS-Chem. *Atmospheric Chemistry and Physics*, *16*(18), 12239–12271. doi: 10.5194/acp-16-12239-2016

Shi, Z., Song, C., Liu, B., Lu, G., Xu, J., Van Vu, T., ... Harrison, R. M. (2021). Abrupt but smaller than expected changes in surface air quality attributable to COVID-19 lockdowns. *Science Advances*, *7*(3). doi: 10.1126/sciadv.abd6696

State Council of the People's Republic of China. (2013). The air pollution prevention and control action plan (2013–2017). , *744*, 140837. Retrieved from `http://www.gov.cn/zwgk/2013-09/12/content_2486773.htm`

Tai, A. P., Mickley, L. J., Jacob, D. J., Leibensperger, E. M., Zhang, L., Fisher, J. A., & Pye, H. O. (2012). Meteorological modes of variability for fine particulate matter (PM2.5) air quality in the United States: Implications for PM2.5 sensitivity to climate change. *Atmospheric Chemistry and Physics*, *12*(6), 3131–3145. doi: 10.5194/acp-12-3131-2012

Tian, R., Ma, X., & Zhao, J. (2021). A revised mineral dust emission scheme in GEOS-Chem: Improvements in dust simulations over China. *Atmospheric Chemistry and Physics*, *21*(6), 4319–4337. doi: 10.5194/acp-21-4319-2021

Travis, K. R., Jacob, D. J., Fisher, J. A., Kim, P. S., Marais, E. A., Zhu, L., ... Zhou, X. (2016). Why do models overestimate surface ozone in the Southeast United States? *Atmospheric Chemistry and Physics*, *16*(21), 13561–13577. doi: 10.5194/acp-16-13561-2016

U.S. Energy Information Agency. (2019). Heat wave results in highest u.s. electricity demand since 2017. , *744*, 140837. Retrieved from `https://www.eia.gov/todayinenergy/detail.php?id=40253`

U.S. Environmental Protection Agency. (2019). National primary and secondary ambient air quality standards. , *744*, 140837. Retrieved from `https://ecfr.federalregister.gov/current/title-40/chapter-I/subchapter-C/part-50`

U.S. Environmental Protection Agency. (2021a). *Air Data: Air Quality Data Collected at Outdoor Monitors Across the US.* Retrieved from `https://aqs.epa.gov/aqsweb/airdata/download_files.html#Meta/`

U.S. Environmental Protection Agency. (2021b). Criteria pollutants national tier 1 for 1970 - 2020. , *744*, 140837. Retrieved from `https://www.epa.gov/air-emissions-inventories/air-pollutant-emissions-trends-data`

Vu, T., Shi, Z., Cheng, J., Zhang, Q., He, K., Wang, S., & Harrison, R. (2019). Assessing the impact of Clean Air Action Plan on Air Quality Trends in Beijing Megacity using a machine learning technique. *Atmospheric Chemistry and Physics*, 1–18. doi: 10.5194/acp-2019-173

Wang, Y. X., McElroy, M. B., Jacob, D. J., & Yantosca, R. M. (2004, nov). A nested grid formulation for chemical transport over Asia: Applications to CO. *Journal of Geophysical Research: Atmospheres*, *109*(D22307). Retrieved from `http://doi.wiley.com/10.1029/2004JD005237` doi: 10.1029/2004JD005237

Wells, B., Dolwick, P., Eder, B., Evangelista, M., Foley, K., Mannshardt, E., ... Weishampel, A. (2021). Improved estimation of trends in us ozone concentrations adjusted for interannual variability in meteorological conditions. *Atmospheric Environment*, *248*, 118234.

Werf, G. R., Randerson, J. T., Giglio, L., Leeuwen, T. T. v., Chen, Y., Rogers, B. M., ... others (2017). Global fire emissions estimates during 1997–2016. *Earth System Science Data*, *9*(2), 697–720.

Wood, S. N. (2011). Fast stable restricted maximum likelihood and marginal likelihood estimation of semiparametric generalized linear models. *Journal of the Royal Statistical Society (B)*, *73*(1), 3-36.

Xie, Y., Wang, Y., Dong, W., Wright, J. S., Shen, L., & Zhao, Z. (2019). Evaluating the Response of Summertime Surface Sulfate to Hydroclimate Variations in the Continental United States: Role of Meteorological Inputs in the GEOS-Chem Model. *Journal of Geophysical Research: Atmospheres*, *124*(3), 1662–1679. doi: 10.1029/2018JD029693

Zhai, S., Jacob, D. J., Wang, X., Liu, Z., Wen, T., Shah, V., ... Liao, H. (2021). Control of particulate nitrate air pollution in China. *Nature Geoscience*, *14*(6), 389–395. doi: 10.1038/s41561-021-00726-z

Zhai, S., Jacob, D. J., Wang, X., Shen, L., Li, K., Zhang, Y., ... Liao, H. (2019). Fine particulate matter (PM 2.5) trends in China, 2013–2018: Separating contributions from anthropogenic emissions and meteorology. *Atmospheric*

*Chemistry and Physics*, *19*(16), 11031–11041.

Zhang, H., Yuan, H., Liu, X., Yu, J., & Jiao, Y. (2018). Impact of synoptic weather patterns on 24h-average PM2.5 concentrations in the North China Plain during 2013–2017. *Science of the Total Environment*, *627*, 200–210. Retrieved from `https://doi.org/10.1016/j.scitotenv.2018.01.248` doi: 10.1016/j.scitotenv.2018.01.248

Zhang, Q., Zheng, Y., Tong, D., Shao, M., Wang, S., Zhang, Y., ... Hao, J. (2019). Drivers of improved PM2.5 air quality in China from 2013 to 2017. *Proceedings of the National Academy of Sciences of the United States of America*, 1–7. doi: 10.1073/pnas.1907956116

Zhang, Y., Vu, T. V., Sun, J., He, J., Shen, X., Lin, W., ... Shi, Z. (2020). Significant Changes in Chemistry of Fine Particles in Wintertime Beijing from 2007 to 2017: Impact of Clean Air Actions. *Environmental Science and Technology*, *54*(3), 1344–1352. doi: 10.1021/acs.est.9b04678

Zhao, Y., Zhang, K., Xu, X., Shen, H., Zhu, X., Zhang, Y., ... Shen, G. (2020). Substantial Changes in Nitrate Oxide and Ozone after Excluding Meteorological Impacts during the COVID-19 Outbreak in Mainland China. *Environmental Science Technology Letters*. doi: 10.1021/acs.estlett.0c00304

Zheng, B., Tong, D., Li, M., Liu, F., Hong, C., Geng, G., ... others (2018). Trends in china's anthropogenic emissions since 2010 as the consequence of clean air actions. *Atmospheric Chemistry and Physics*, *18*(19), 14095–14111.

Zhong, Q., Ma, J., Shen, G., Shen, H., Zhu, X., Yun, X., ... Tao, S. (2018). Distinguishing Emission-Associated Ambient Air PM2.5 Concentrations and Meteorological Factor-Induced Fluctuations. *Environmental Science and Technology*, *52*(18), 10416–10425. doi: 10.1021/acs.est.8b02685

Zurbenko, I. G. (1994). Detecting and tracking changes in ozone air quality. *Air and Waste*, *44*(9), 1089–1092. doi: 10.1080/10473289.1994.10467303

## Supplementary methods

### Implementation of LASSO and RF

As the incorporation of both local and regional features can quickly expand the dimensionality of the feature space, we use the Least Absolute Shrinkage and Selection Operator (LASSO) and the Random Forest (RF) model to assess the importance of regional meteorological features. Both methods are commonly-used approach with good prediction performances with high dimensional data inputs, and are thus appropriate for the analysis with a large number of regional meteorological features. For these two methods, we rewrite equation 1 as the following:

$$y_{it} = \beta_i^{obs} \times t + g_i(X_{it}, Z_t, W_t) + \epsilon_{it} \tag{4}$$

where $g_i()$ denotes the functional form fitted by LASSO or RF. $X_{it}$ again denotes the local meteorology features for grid cell $i$ on day $t$. $Z_t$ denotes the regional scale meteorology features including the meteorological features for all grid cells in the US on day $t$ (98 cells in 4×5 degrees; we choose a relatively coarse resolution due to computational cost). Meteorological information in each location in the US may help explain the pollutant concentrations in grid cell $i$. In total, we have 10 local features ($X_{it}$) and 10×98=980 regional scale features ($Z_t$). $W_t$ denotes the day and month variable to model the daily and monthly variability in pollutant that are unrelated to meteorological variability. For LASSO, we use month-of-year×day-of-month fixed effect (same as all the other methods except for RF), and these fixed effects are not penalized in the LASSO regression. For RF, we use the month-of-year variable (from 1 to 12), and day-of-month variable (from 1 to 31), due to the inefficient performance of RF working with large number of fixed effects. Thus, the difference between RF and the other methods may also come from the different choice of modeling monthly and daily variability.

The coefficient $\beta_i^{obs}$ is obtained with the following procedure using the double machine learning approach by Chernozhukov et al. (2018).

(1) We first partition the time series of {$y_{it}$, $X_{it}$, $Z_t$, $W_t$} into 4 folds. We use 75% of the data as training data and the remaining 25% for predictions. We train the following two models on the training data:

$$y_{it} = f(X_{it}, Z_t, W_t)$$
$$t = g(X_{it}, Z_t, W_t)$$

(2) We then apply models $f(.)$ and $g(.)$ to the prediction set to get predictions of $y_{it}$ and $t$ for the rest 25% of the data. The above process is repeated four times to derive predictions for the entire time series (predictions denoted as $\widehat{y_{it}}$ and $\widehat{t}$).

(3) We calculate the residuals of each model $\widetilde{y_{it}} = y_{it} - \widehat{y_{it}}$ and $\widetilde{t} = t - \widehat{t}$. The coefficient of interest $\beta_i^{obs}$ is then calculated as:

$$\beta_i^{obs} = \frac{\sum_t \widetilde{t}\widetilde{y_{it}}}{\sum_t \widetilde{t}\widetilde{t}}$$

this is equivalent to setting up a linear regression of $\widetilde{y_{it}} \sim \widetilde{t}$ and obtain the slope coefficients (as shown by Chernozhukov et al. (2018)).

The hyper-parameters of RF and LASSO are tuned with 4-fold cross validation. We also perform two sensitivity analyses: 1) with a different spatial resolution of the regional scale features (2×2.5 degrees instead of 4×5 degrees), and 2) with different numbers of folds to estimate the trend coefficients. Our results are similar across these sensitivity analyses (see figure S15).

The double machine learning framework involves a sample partition procedure (steps (1) and (2) above). This procedure, however, does not fit the purpose of including time fixed effects in the LASSO model (as randomly partitioned training and test sets could have very unbalanced number of observations from a given month-day pair). Therefore, step (1) and (2) are only implemented for the RF model, and coefficients of the LASSO model is directly derived from step (3) without sample splitting. This is okay for the LASSO model as the risk of "overfitting" has already been eliminated by using the tuned penalizing factor (i.e. the hyper-parameters) derived from a 4-fold cross-validation.

887 ## SI tables and figures

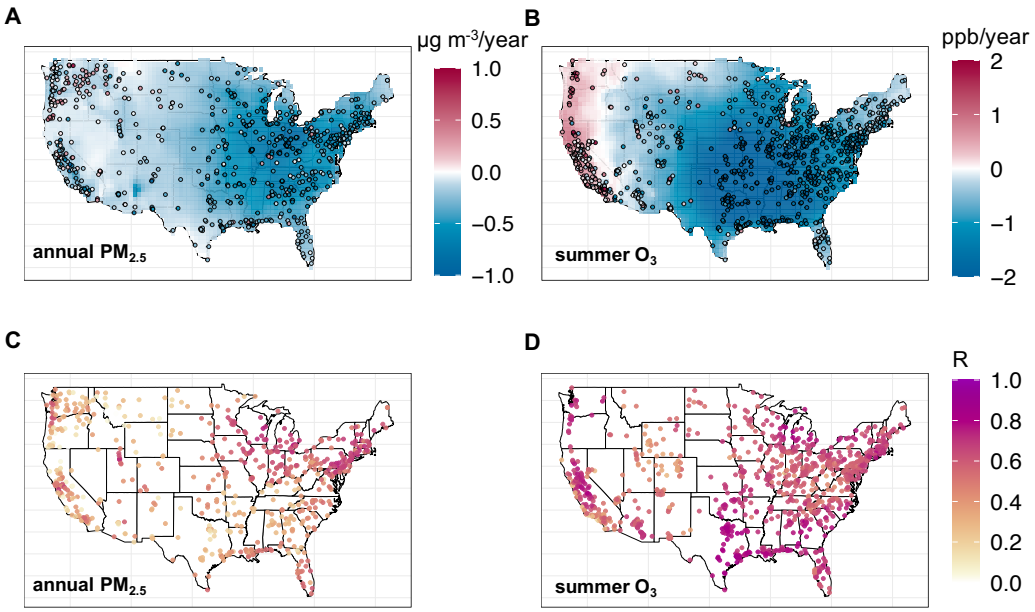


Figure S1: Comparison between the annual $PM_{2.5}$ (Panels A and C) and summer $O_3$ (Panels B and D) concentrations measured by the monitoring network and GEOS-Chem simulations in the US (2011-2017). Panels A and B show the trends in monitored concentrations (dots) and trends in the observational scenarios in GEOS-Chem simulations (background) without meteorology corrections. Panels C and D show the Pearson correlation coefficient ($R$) between the daily measured concentrations and simulated concentrations.

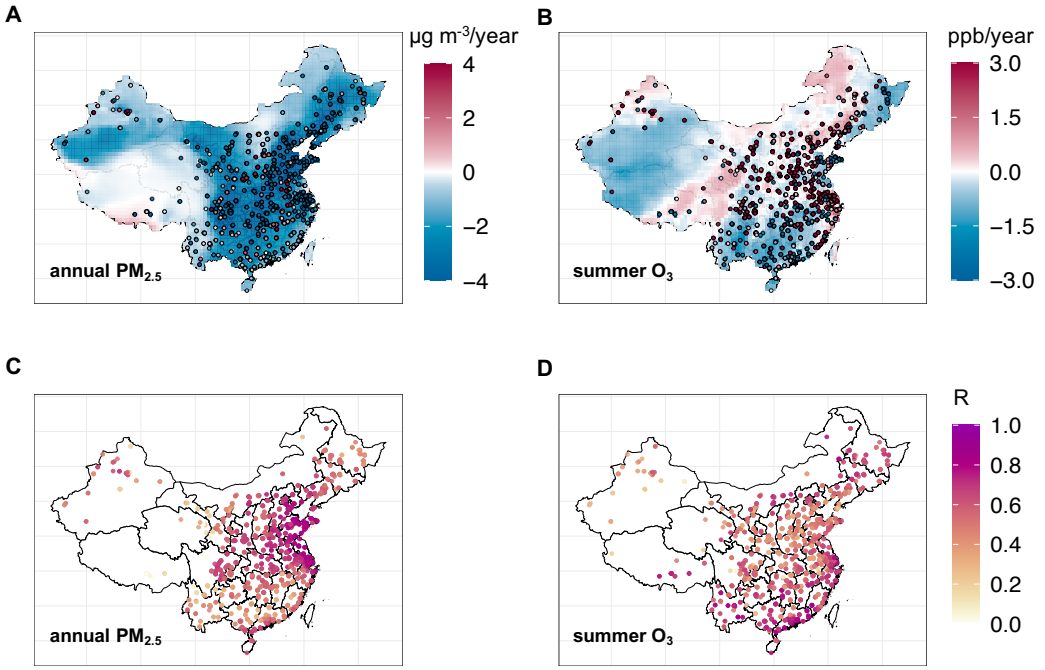


Figure S2: Comparison between the annual $PM_{2.5}$ (Panels A and C) and summer $O_3$ (Panels B and D) concentrations measured by the surface monitoring network and GEOS-Chem simulations in China (2014-2017). Panels A and B show the trends in monitored concentrations (dots) and trends in the observational scenarios in GEOS-Chem simulations (background) without meteorology corrections. Panels C and D show the Pearson correlation coefficient ($R$) between the daily measured concentrations and simulated concentrations.

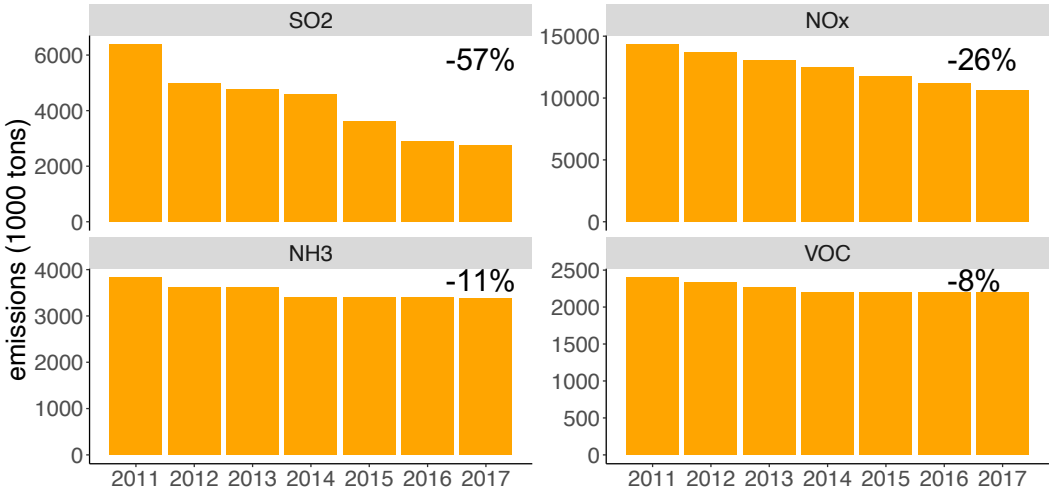


Figure S3: National total anthropogenic emissions in the US (2011- 2017). The emissions data is derived from the national total emissions of criterion air pollutants reported by the US EPA Air Emissions Inventory.

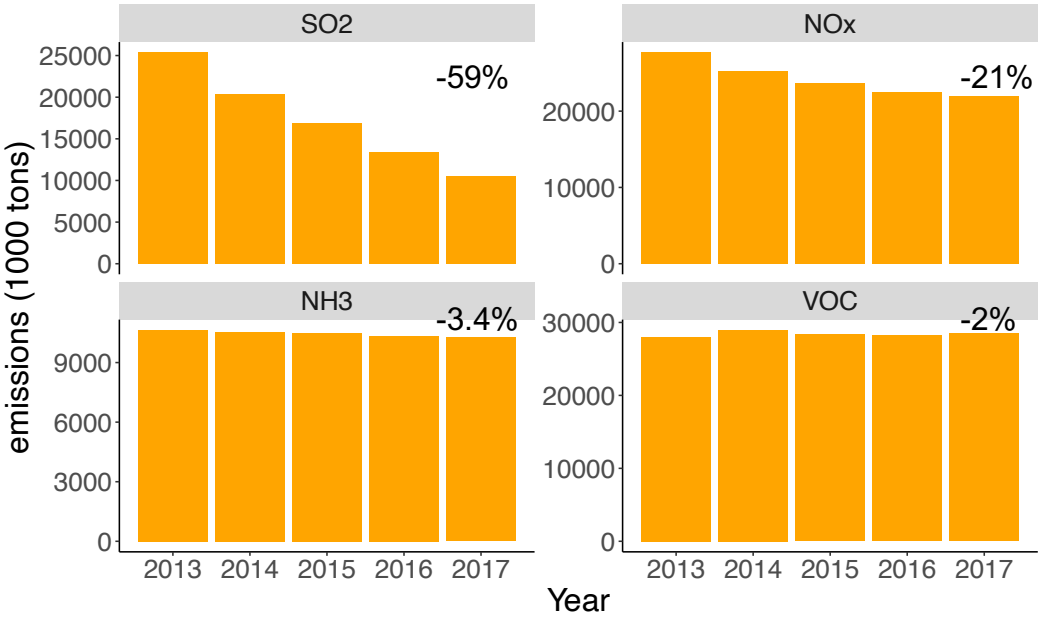


Figure S4: National total anthropogenic emissions in China (2013- 2017). The emissions data is derived from the Multi-resolution Emission Inventory (MEIC).

| Model | Annual $PM_{2.5}$ in the US | | | Summer $O_3$ in the US | | |
|---|---|---|---|---|---|---|
| | average error | median relative error | cells with relative error >50% | average error | median relative error | cells with relative error >50% |
| No correction | 0.066 | 28% | 27% | 0.67 | 154% | 84% |
| MLR (5 features) | 0.092 | 43% | 44% | 0.38 | 84% | 71% |
| MLR (10 features) | 0.083 | 40% | 40% | 0.33 | 71% | 64% |
| Quadratic | 0.088 | 40% | 42% | 0.29 | 60% | 58% |
| Cubic | 0.075 | 39% | 41% | 0.28 | 60% | 58% |
| Spline | 0.076 | 40% | 41% | 0.28 | 61% | 59% |
| GAM | 0.076 | 40% | 43% | 0.29 | 61% | 58% |
| RF-local | 0.067 | 33% | 39% | 0.34 | 78% | 70% |
| LASSO-regional | 0.078 | 31% | 33% | 0.31 | 68% | 65% |
| RF-regional | 0.047 | 25% | 23% | 0.19 | 46% | 47% |

Table S1: Estimation errors of trend estimates in the US under different correction methods. The average estimation errors, median relative error, and fraction of grid cells with relative error greater than 50% are shown in the table. Relative errors are calculated as the ratio of estimation error to the trend estimate in the counterfactual scenario. MLR (5 features) only use temperature, precipitation, humidity, and surface wind speed (U,V directions) as the meteorological features.

| Model | Annual $PM_{2.5}$ in China | | | Summer $O_3$ in China | | |
|---|---|---|---|---|---|---|
| | average error | median relative error | cells with relative error >50% | average error | median relative error | cells with relative error >50% |
| No correction | 0.89 | 224% | 77% | 0.43 | 95% | 74% |
| MLR (5 features) | 1.07 | 193% | 80% | 0.42 | 90% | 68% |
| MLR (10 features) | 0.90 | 159% | 79% | 0.41 | 85% | 68% |
| Quadratic | 1.00 | 142% | 82% | 0.36 | 76% | 62% |
| Cubic | 1.07 | 143% | 82% | 0.34 | 68% | 59% |
| Spline | 1.08 | 140% | 84% | 0.33 | 69% | 59% |
| GAM | 1.06 | 139% | 82% | 0.35 | 72% | 59% |
| RF-local | 0.99 | 172% | 82% | 0.31 | 64% | 58% |
| LASSO-regional | 0.83 | 184% | 75% | 0.46 | 98% | 73% |
| RF-regional | 0.64 | 152% | 67% | 0.28 | 61% | 58% |

Table S2: Estimation errors of trend estimates in China under different correction methods. The average estimation errors, median relative error, and fraction of grid cells with relative error greater than 50% are shown in the table. Relative errors are calculated as the ratio of estimation error to the trend estimate in the counterfactual scenario. MLR (5 features) only use temperature, precipitation, humidity, and surface wind speed (U,V directions) as the meteorological features.

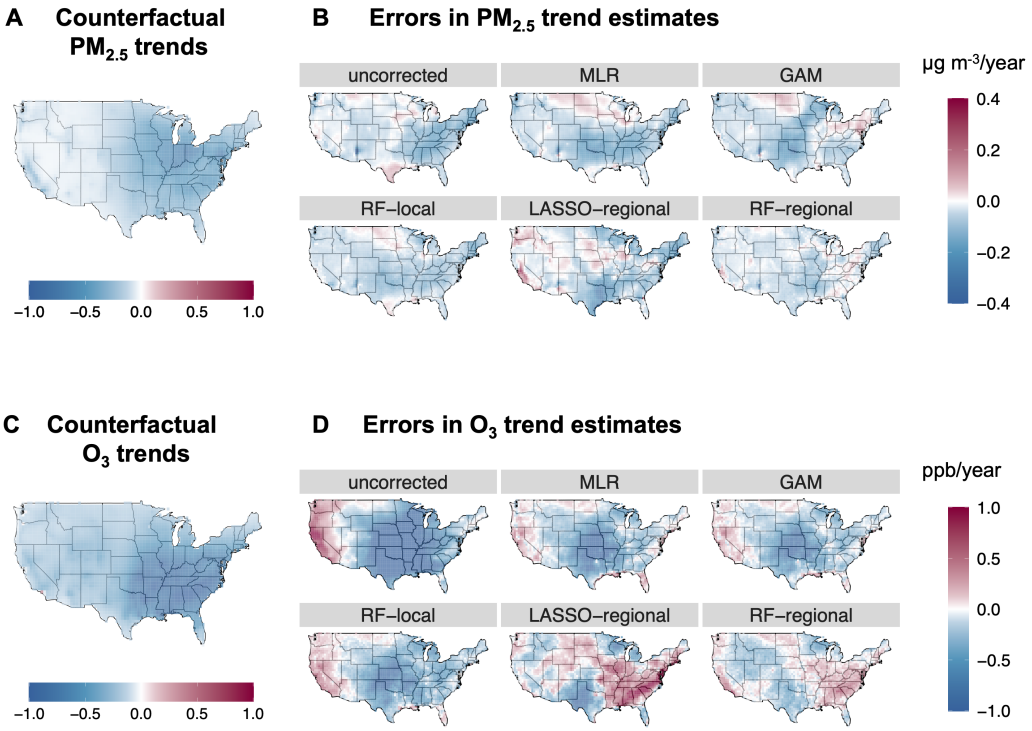


Figure S5: Trend estimates of daily annual $PM_{2.5}$ (Panels A and B) and summer $O_3$ (C and D) in the US. Panels A and C show trend estimates under the counterfactual scenario ($\beta^{count}$). Panels B and D show the estimation errors of trend estimates under different correction methods compared with the counterfactual scenarios ($\beta^{obs} - \beta^{count}$). The average of the absolute error for each method is shown in the figure. Unit of trend estimate is $\mu$g m$^{-3}$/year for $PM_{2.5}$ or ppb/year for $O_3$.

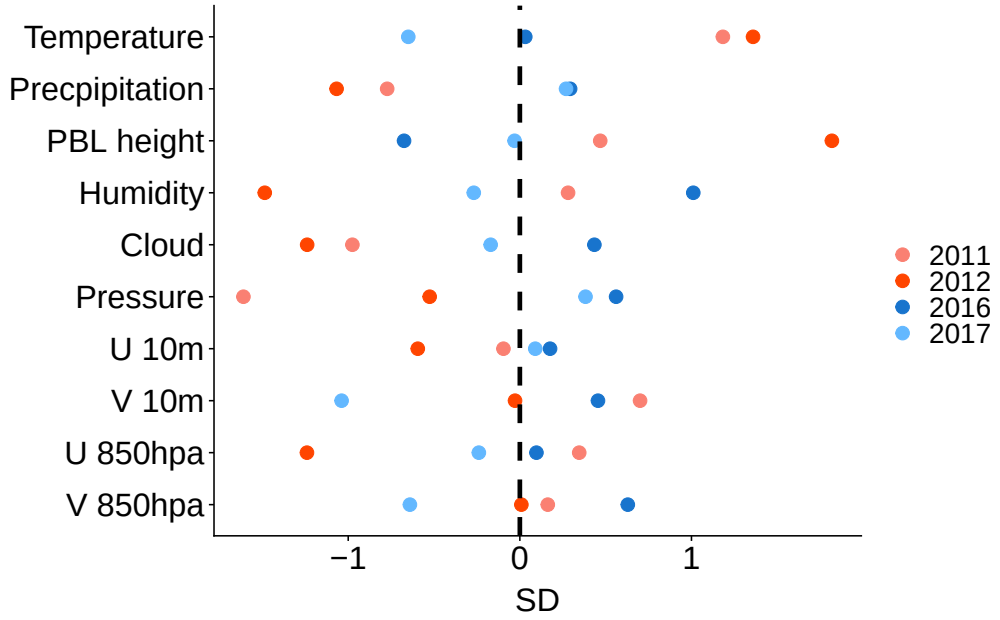


Figure S6: Deviations of meteorological features from the 7-year average in the US (South and Midwest). The deviation is quantified in the units of standard deviation (SD) across the 7-year period. Zero indicates the 7-year average. This plot shows the summer time average of daily MDA8 meteorological variables for each year aggregated over South and Midwest US.

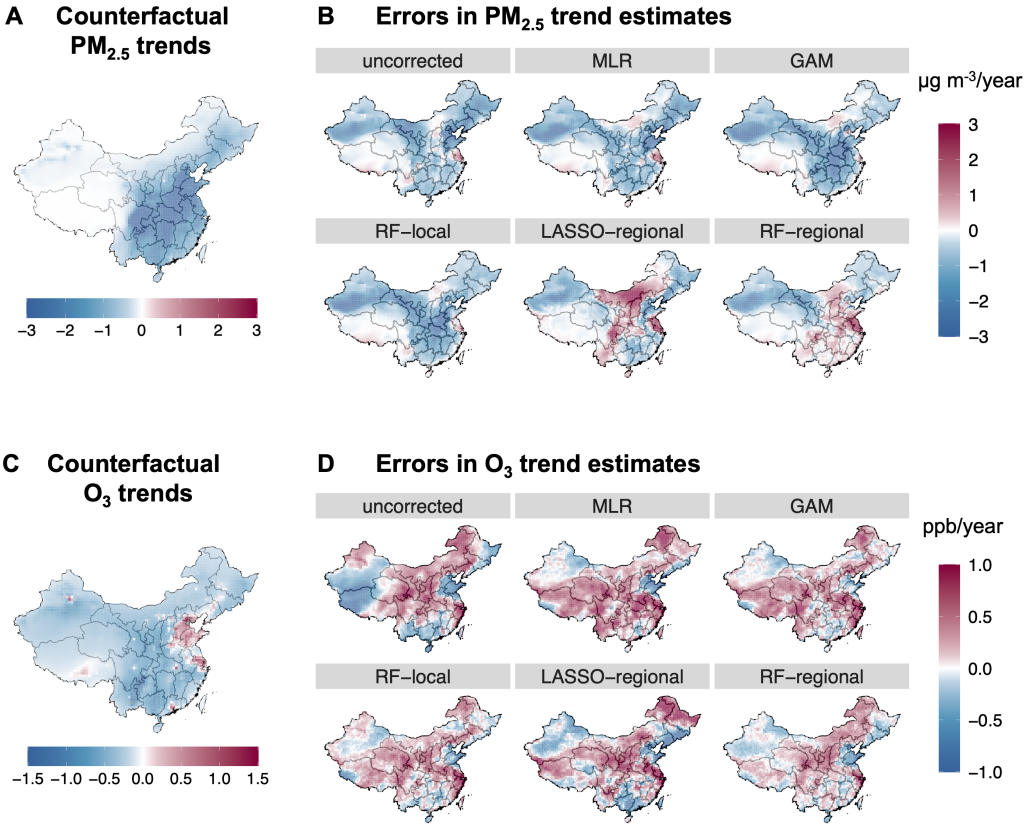


Figure S7: Trend estimates of daily annual $PM_{2.5}$ (Panels A and B) and summer $O_3$ (C and D) in China. Panels A and C show trend estimates under the counterfactual scenario ($\beta^{count}$). Panels B and D show the estimation errors of trend estimates under different correction methods compared with the counterfactual scenarios ($\beta^{obs} - \beta^{count}$). The average of the absolute error for each method is shown in the figure. Unit of trend estimate is $\mu$g m$^{-3}$/year for $PM_{2.5}$ or ppb/year for $O_3$.

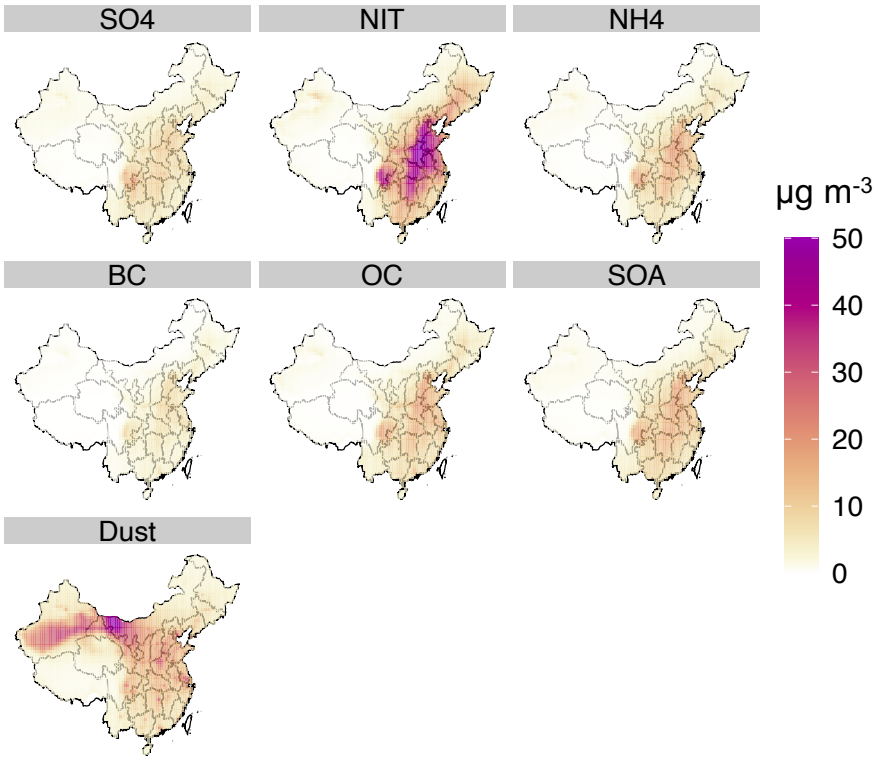


Figure S8: Concentrations of component species of $PM_{2.5}$ in China (average across 2013-2017). The figure shows concentrations of sulfate ($SO_4$), nitrate (NIT), ammonium ($NH_4$), black carbon (BC), organic carbon (OC), secondary organic aerosol (SOA) and dust.

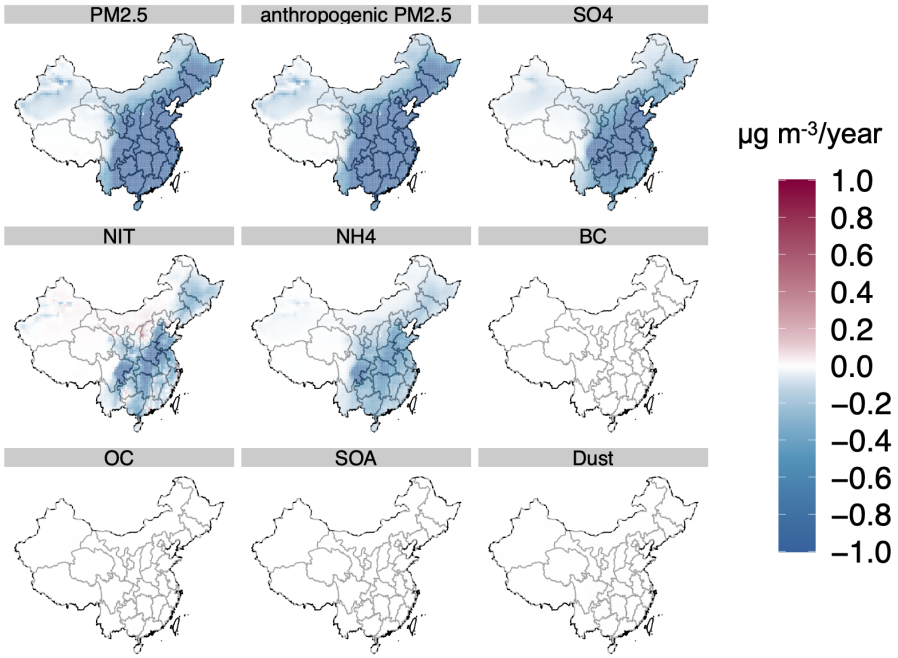


Figure S9: Counterfactual trends of component species of $PM_{2.5}$ in China. The figure shows counterfactual trends of total $PM_{2.5}$, anthropogenic $PM_{2.5}$ (total $PM_{2.5}$ excluding dust and sea salt), sulfate ($SO_4$), nitrate (NIT), ammonium ($NH_4$), black carbon (BC), organic carbon (OC), secondary organic aerosol (SOA) and dust.

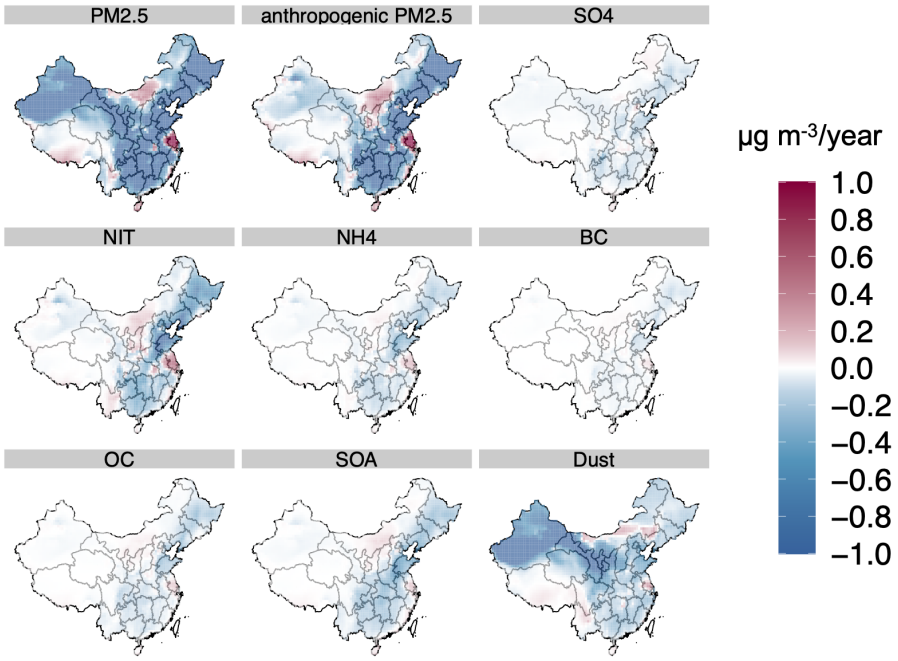


Figure S10: Differences between counterfactual trends and trends evaluated under MLR ($\beta^{MLR} - \beta^{count}$) of component species of $PM_{2.5}$ in China. The figure shows estimation errors of total $PM_{2.5}$, anthropogenic $PM_{2.5}$ (total $PM_{2.5}$ excluding dust and sea salt), sulfate ($SO_4$), nitrate (NIT), ammonium ($NH_4$), black carbon (BC), organic carbon (OC), secondary organic aerosol (SOA) and dust.

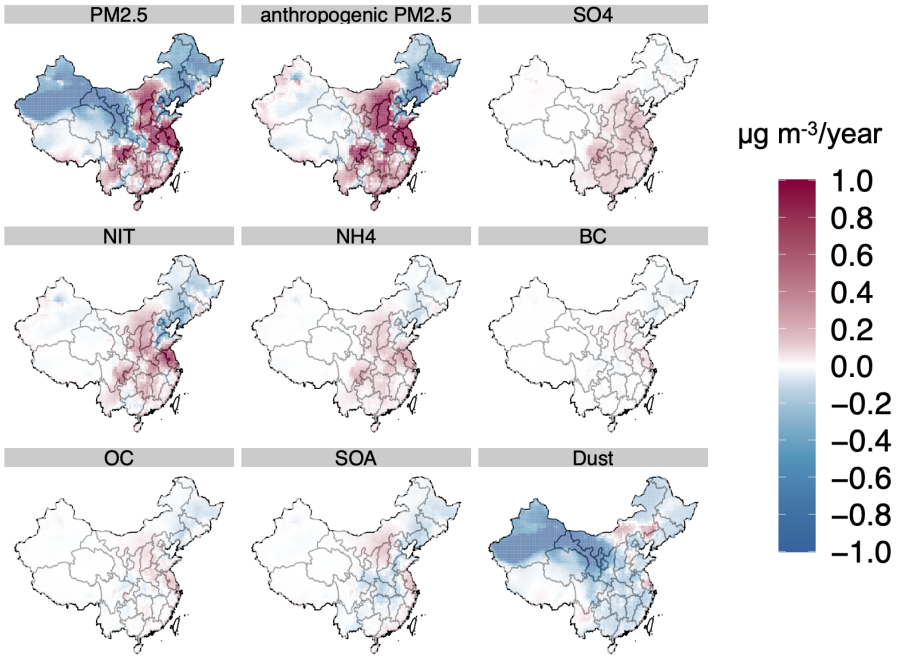


Figure S11: Differences between counterfactual trends and trends evaluated under RF-regional ($\beta^{RF-regional} - \beta^{count}$) of component species of $PM_{2.5}$ in China. The figure shows estimation errors of total $PM_{2.5}$, anthropogenic $PM_{2.5}$ (total $PM_{2.5}$ excluding dust and sea salt), sulfate ($SO_4$), nitrate (NIT), ammonium ($NH_4$), black carbon (BC), organic carbon (OC), secondary organic aerosol (SOA) and dust.

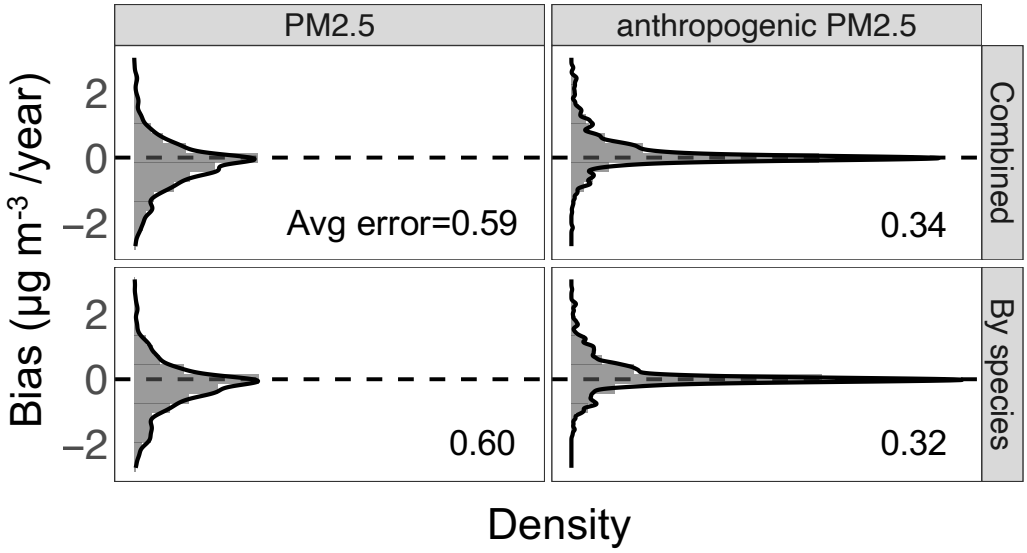


Figure S12: Histograms of the estimation errors of trend estimates of annual $PM_{2.5}$ in China under two implementations of the *RF-regional* method. The upper panels (Combined) show results of fitting RF models to the combined concentrations of $PM_{2.5}$ to directly estimate trends (the main results). The lower panels (By species) show results of fitting RF models to individual $PM_{2.5}$ species and then combine predictions to estimate trends. The left panels show results for total $PM_{2.5}$ and right panels show results for the anthropogenic $PM_{2.5}$. The average estimation errors for each implementation is shown in the figure.

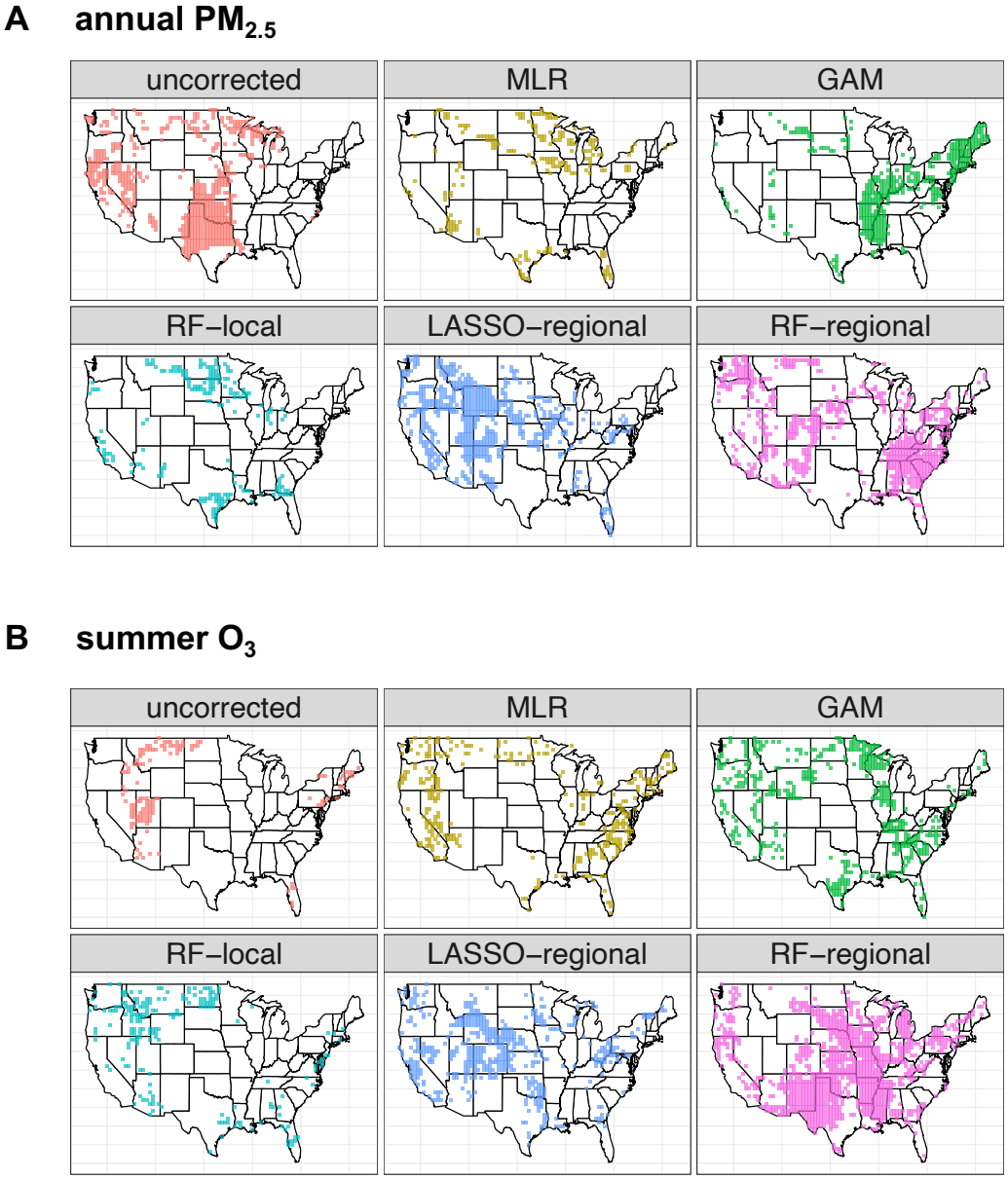


Figure S13: This figure shows which method estimates a trend closest to the trend estimate in the counterfactual scenario for each grid cell.

**A annual $PM_{2.5}$**

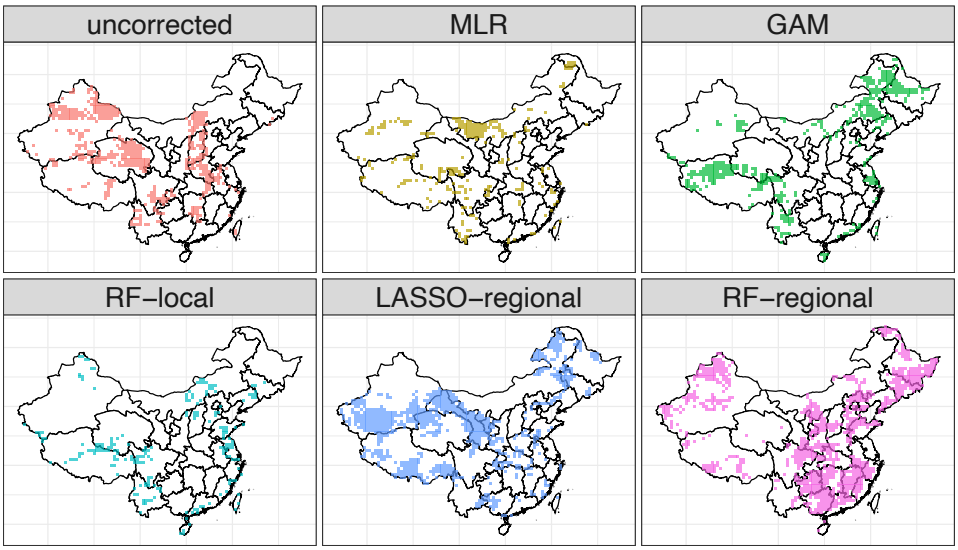


**B summer $O_3$**

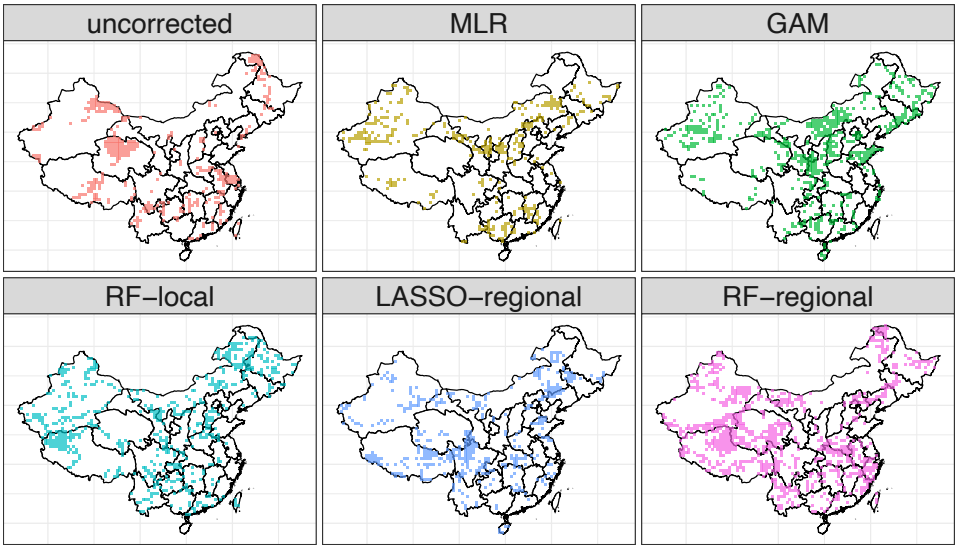


Figure S14: This figure shows which method estimates a trend closest to the trend estimate in the counterfactual scenario for each grid cell.

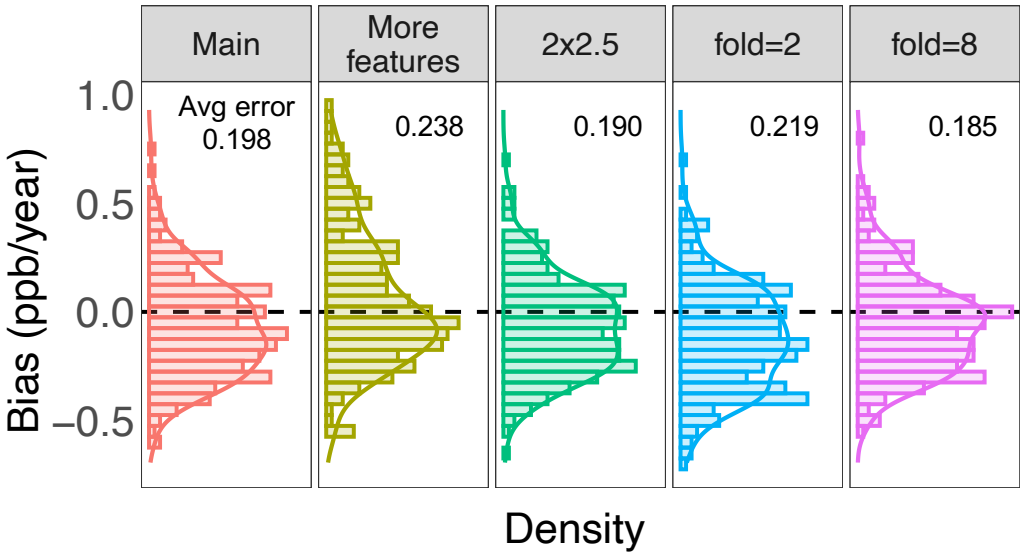


Figure S15: Histograms of the estimation errors of trend estimates of summer $O_3$ in the US under different implementations of the *RF-regional* method. From left to right: Main (the main results), More features (includes 9 extra meteorological features), 2x2.5 (uses regional features with spatial resolution of $2\times2.5°$, instead of $4\times5°$), fold=2 (uses 2 folds for data-splitting and cross-fitting), fold=8 (uses 8 folds for data-splitting and cross-fitting). The average of the absolute error for each implementation is shown in the figure. This figure only uses a random subset of all the grids in the US due to the computational cost.